Earth Chemistry and Materials

(updated January 2006)

Cin-Ty A. Lee
Rice University

Chapter 1
Introduction

1.1 Why study rocks?

I am a petrologist and I study rocks. Petrology is the study of how rocks form (rocks being defined as a natural assemblage of individual minerals). More specifically, petrologists seek the physical and chemical conditions necessary for the formation and modification of certain types of rocks. On one level, petrology involves the art of identifying and classifying different minerals and rock types into some sort of petrogenetic context. By petrogenesis, what we mean is some sort of model or theory about the physical and chemical processes by which a particular rock or group of rocks formed or evolved. This leads naturally to the second level on which petrologists operate, that is, petrologists must bring together principles from physics and chemistry to develop petrogenetic models that are consistent with observation. The predictions resulting from any such models should then be tested by returning to the rocks or by reproducing certain processes in laboratory experiments. It is through this culmination of physical and chemical principles in the context of rocks that we as Earth scientists can eventually unravel larger scale processes, such as ore formation, continent formation, evolution of the Earth and other planets, and so forth.

The approach we will take in these lecture notes will be to focus first on processes and then come back to rock classification in the context of processes. This is of course the reverse of the historical development of petrology. I have chosen this approach because all too often I have heard from my non-petrology colleagues that petrology seems like an exercise in somewhat arbitrary classifications accompanied by unnecessarily dense terminology. There is of course some truth to these statements, but there is actually some method to this madness and it is this method that I would like to get across here. Perhaps by developing an initial appreciating of the processes by which rocks are formed and how they relate to the origin and evolution of our planet, we can then develop a better appreciation for the rock record itself.

So let's begin with what rocks might tell us. A few simple definitions are in order. Rocks can be classified as igneous, metamorphic and sedimentary origin. *Igneous rocks* form by the direct solidification of magma (*molten rock*). *Metamorphic rocks* represent the integrated end-product of all processes that impart a mineralogical, textural and/or chemical transformation (e.g., metamorphosis) of an igneous, sedimentary or metamorphic rock into a different rock. *Sedimentary rocks* are the lithified products of sediments. Sediments represent all loose solid materials that accumulate at the surface of the Earth, with the loose particles making up sediments being derived from physical or chemical weathering of pre-existing rocks, direct chemical precipitation from water, and/or organisms' skeletal remains.

Dividing the field of petrology into these sub-categories helps to simplify the content for teaching purposes. In reality, however, each of the rock-forming processes - igneous, metamorphic, and sedimentary- is intimately linked as they are all components within the rock cycle. To illustrate, we can simplify the Earth into a number of sub-reservoirs, i.e. large, coherent regions of mass characterized by a distinctive composition. The most obvious Earth reservoirs are the atmosphere, oceans, and the solid part of the Earth, which itself can be subdivided into continental crust, oceanic crust, mantle and metallic core (Fig. 1.1 and Table

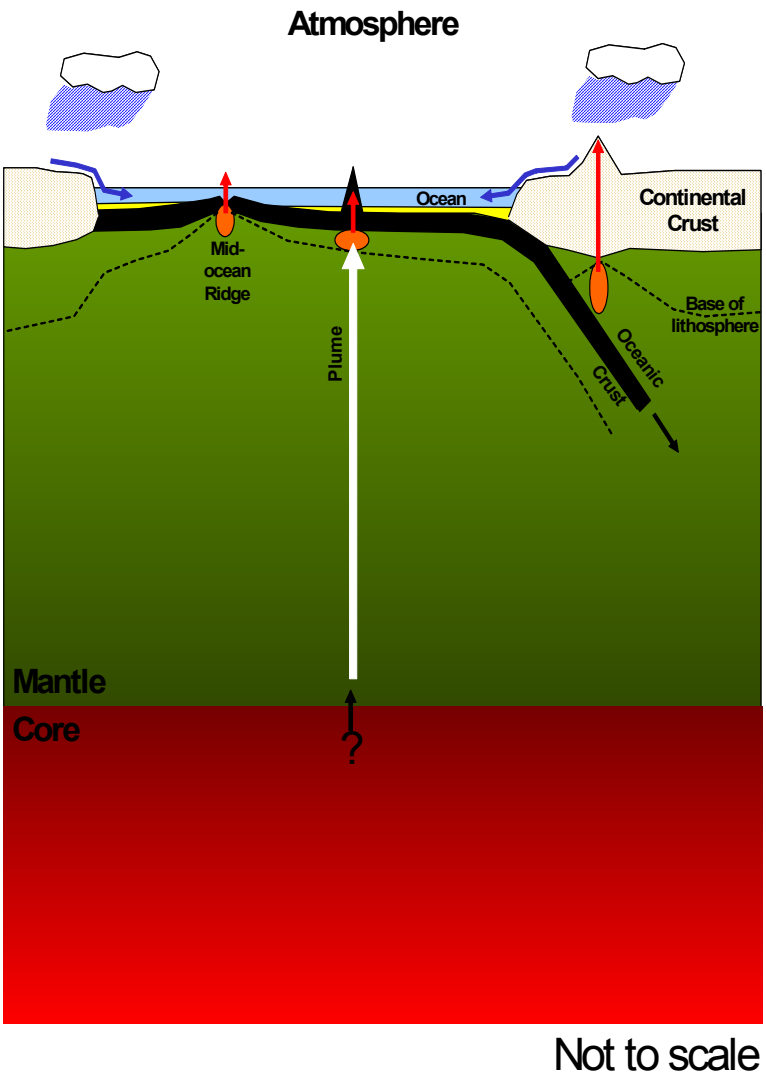

Figure 1.1. Schematic diagram showing some of the major reservoirs in the Earth (atmosphere, ocean, continental crust, oceanic crust, mantle, core) and how they may interact. Red ovals represent regions where solid mantle is being partially melted.

1.1). That each of these reservoirs exists reflects the fact that the Earth has been unmixing (differentiating) ever since it was formed. Each of these reservoirs is continually evolving in size and composition as each reservoir interacts with each other or in other words mixes back together. For example, there is a net contribution of material from the mantle to the atmosphere, ocean, continental crust and oceanic crust: degassing at mid-ocean ridges or arcs releases magmatic gases to the atmosphere and oceans, hydrothermal fluxing at mid-ocean ridges results in the net flux of certain chemical components into the ocean, and magmatism at mid-ocean ridges and arc volcanoes result in the addition of new mass to oceanic and continental crust (Figs. 1.1 and 1.2). In addition, physical and chemical weathering of continental crust results in the transport of sediments to the seafloor, some of which are ultimately recycled along with oceanic crust back into the mantle at subduction zones. These examples represent only part of

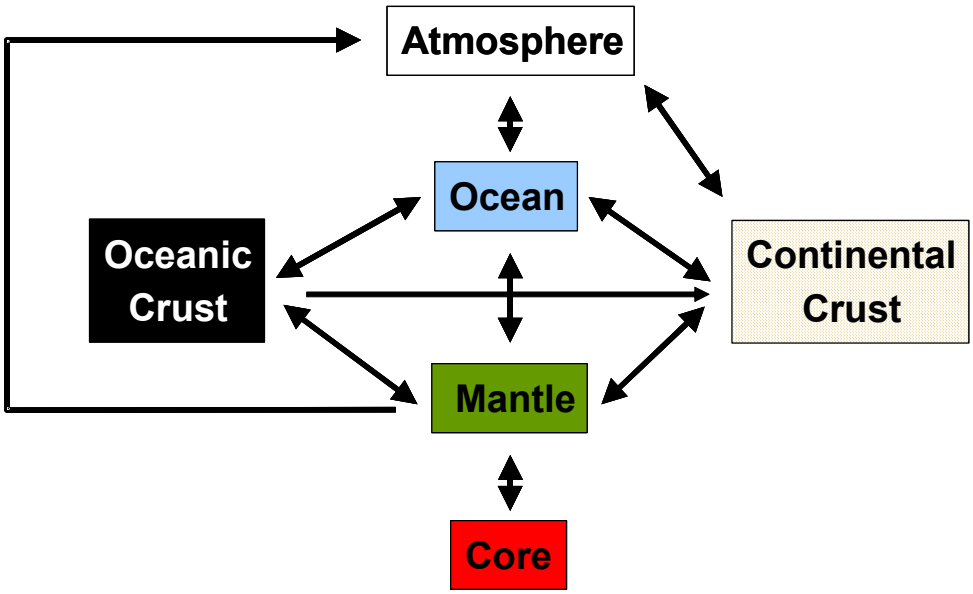

Figure 1.2. Earth systems cycles. A simplified subdivision of the Earth into its major reservoirs and how they interact with each other. Arrows reflect direction of

all the different ways in which these reservoirs can interact with each other (Figs. 1.1 and 1.2). In trying to decipher how the nature of the Earth has evolved through time, it is necessary to quantitatively describe the physical and chemical processes represented by each of the arrows, and moreover, how the system as a whole or its subsystems have changed.

In this treatise, we will cover the fundamental principles of igneous, metamorphic and sedimentary petrology in the broader context of the rock cycle and the driving forces that allow for chemical and physical differentiation of the Earth into its major rocky reservoirs. We will

Table 1.1. Some physical properties of the Earth

Mean radius (km)	6371.01		
Total surface area (km^2)	5.10×10^8		
Oceanic surface area (km^2)	3.62×10^8		
Volume (km^3)	1.08×10^{12}		
Mass (kg)	5.97×10^{24}		
Mean density (g/cm^3)	5.52		
Core radius (km)	3485		
	Mass (kg)	% of Whole Earth	% of Bulk Silicate Earth
Total atmosphere	5.14×10^{18}	8.65×10^{-5}	
Hydrosphere	1.66×10^{21}	0.0279	0.0413
Total Crust	2.37×10^{22}	0.3951	0.585
Continental crust	1.52×10^{22}	0.25	0.38
Oceanic crust	8.45×10^{21}	0.14	0.21
Mantle	4.01×10^{24}	67.08	99.37
Bulk Silicate Earth	4.03×10^{24}	67.51	
Core	1.94×10^{24}	32.5	

Data are from [*Lodders and Fegley*, 1998]

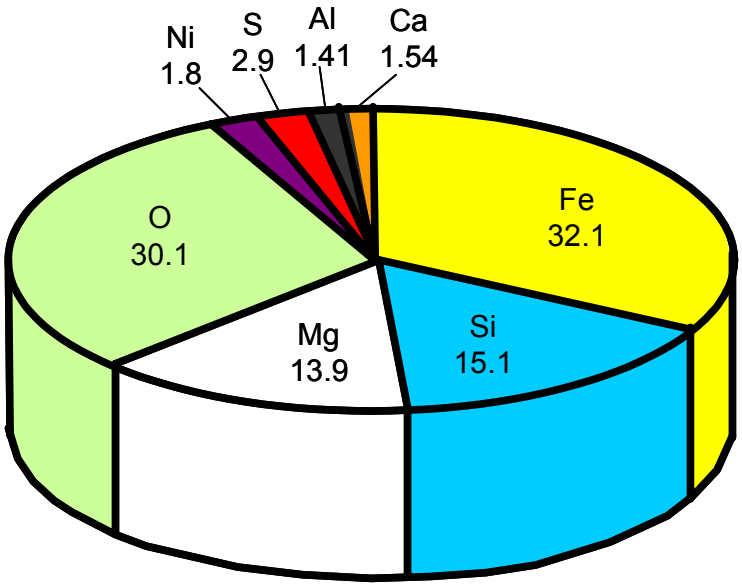

Figure 1.3. Relative atomic abundances of the eight most common elements that comprise 99% of the mass of the solid Earth.

not discuss processes that are internal to the ocean and atmosphere, but we will end our journey through petrology by ultimately linking the solid Earth reservoirs to the ocean and atmosphere.

1.2 Composition of the solid Earth

The solid part of the Earth (e.g., the metallic core and rocky crust and mantle) is predominantly made up of O (~30 wt. %), Fe (~32%), Mg (~14%), Si (~15%), Ca (1.5%), and Al (1.4%), as shown in Figure 1.4. Most of the Fe is in the core, which makes up ~32.5 wt. % of the entire Earth. This leaves the rocky outer part of the Earth with ~44% O, ~23% Mg, ~21% Si, 2.5% Ca and 2.4% Al. Thus, the outer part of the Earth is dominated by Si and O and is accordingly dominated by silicate minerals[1].

It is likely that the outer part of the Earth, the *bulk silicate Earth*, was more or less compositionally homogeneous during its earliest history because the oldest known rocks are only ~4.1 Ga old (the age of the Earth is 4.55 Ga), indicating that whatever rocks were created at the Earth's surface during the first ~0.5 Ga were efficiently rehomogenized in the bulk silicate Earth. It is clear now that the bulk silicate Earth has subsequently differentiated into various subreservoirs. The most striking subreservoirs are the continental crust and oceanic crust. Continental crust is on average ~35 km thick and makes up ~0.38 % by mass of the bulk silicate Earth. Oceanic crust averages ~7-10 km thick and makes up ~0.2 % by mass of the bulk silicate Earth. The remaining 99.4 % of the bulk silicate Earth is the mantle, which consists of that part of the mantle that is residual to the extraction of continental and oceanic crust, any primitive (e.g., undifferentiated) parts retaining bulk silicate Earth compositions, and any crustal components that may have been recycled back into the mantle by subduction or related processes.

[1] Silicates are compounds based on the silica tetrahedron, in which a Si is surrounded by four O atoms.

Table 1.2 shows the average compositions of these differentiated reservoirs. A striking difference is that continental crust is considerably enriched in Si and Al compared to the bulk silicate Earth. This difference is manifested in contrasting mineralogies: the continental crust is principally made up of quartz (SiO_2), feldspars ($KAlSi_3O_8$) and some mafic (mafic = Mg, Fe, and Ca-rich) minerals, such as hornblende and/or biotite; the mantle being enriched in Mg and Fe relative to continental crust is accordingly dominated by mafic minerals, such as olivine ($(Mg,Fe)_2SiO_4$) and pyroxene ($(Ca,Mg,Fe)_2Si_2O_6$), but no quartz. As we will learn later, an even more striking observation is that the continental crust, despite its extremely small relative mass, contains most of the highly incompatible trace elements in the Earth, such as Cs, Rb, Ba, U, Th, and K (estimates range from 50 to 90%). U, Th, and K are radioactive elements, and their high abundance in the continental crust indicates that internal heat production in the Earth associated with radioactive decay has been gradually migrating towards the surface of the Earth in direct correlation with the rate of continental crust formation.

We are thus left with a myriad of questions. What processes dictate how the Earth unmixes, i.e. differentiates? In this context, we are concerned with not only the processes that control chemical mass transfer during differentiation, but also the physical processes of differentiation. How does the mantle melt? What conditions dictate the composition of the melt and how does the melt evolve in composition as it cools? How does tectonic environment control the nature of differentiation? How is melt transported from its source region to the crust? What processes allow for recycling of crustal material back into the mantle? What chemical changes occur during crustal recycling? Can we quantify how these differentiation processes and their rates have evolved through time?

There is no doubt that answering these questions have and will continue to improve our understanding of problems in global tectonics, mantle and crustal geodynamics, Earth systems history, planetary geology, and even, economic geology (i.e., the study of economic ore deposits). However, in order to pursue these questions from a petrologist's viewpoint, it will be necessary to master a number of tools in the modern petrologist's toolbox (Figure 1.3). This

Table 1.2. Comparative chemistries of different Earth reservoirs

	Bulk Silicate Earth[1]	Continental Crust[2]	Oceanic crust	
			Most primitive basaltic glass[3]	Calculated primary composition[4]
MgO (wt. %)	36.33	4.4	10.1	17.81
Al_2O_3 (wt. %)	4.73	15.8	16.4	12.08
SiO_2 (wt. %)	45.56	59.1	49.7	47.85
CaO (wt. %)	3.75	6.4	13.0	11.22
FeO^T (wt. %)	8.17	6.6	7.9	8.98
Mg#	0.888	0.543	0.695	0.780

[1][*O'Neill and Palme*, 1998]
[2][*Rudnick*, 1995]
[3][*Frey et al.*, 1974]
[4][*Elthon*, 1979]
Mg# = molar Mg/(Mg+Fe); FeO^T is total Fe^{2+} and Fe^{3+}

treatise will cover the fundamentals of chemical thermodynamics, mineral physical chemistry, trace-element geochemistry, radiogenic and non-radiogenic isotope geochemistry, kinetic theory, and basic fluid dynamics pertinent to magma transport. Every attempt will be made to link theory to observations, such as petrographic and field examples, insofar as it is possible to write about field observations!

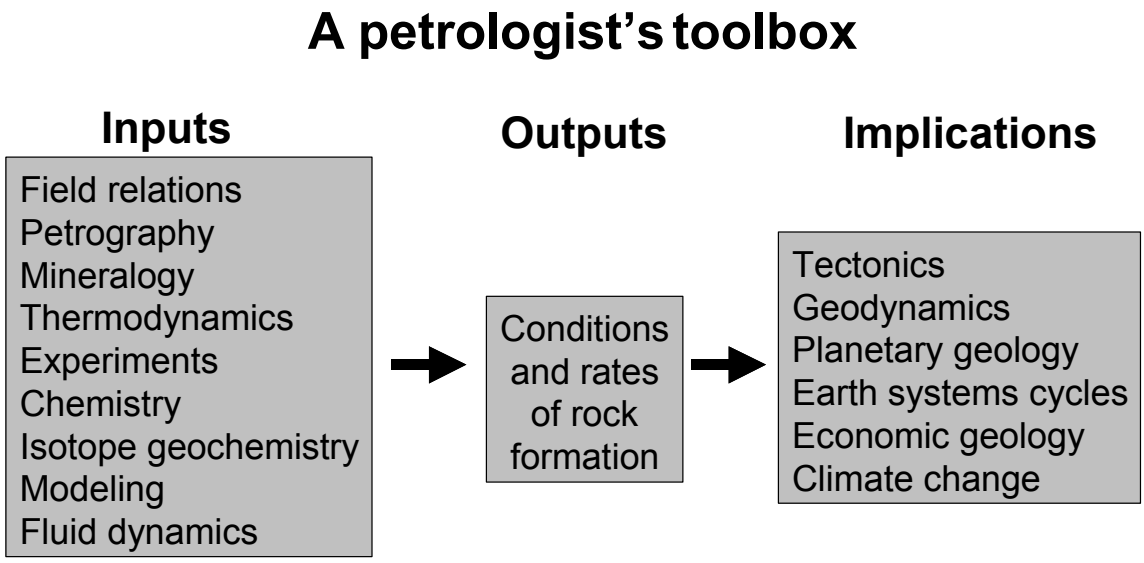

Figure 1.3 Diagram showing the tools of a modern petrologist in relation to the goals of petrology.

Chapter 2
From accretion of the Earth to plate tectonics

2.1 Making the bulk Earth

2.1.1 The Earth has an iron core

In Chapter 1, we briefly touched on the composition of the bulk Earth, but how is the bulk Earth composition determined? There is presently no rock sample that has a representative bulk Earth composition as the Earth has been grossly differentiated. The first hint that the Earth might be radially heterogeneous came as early as the 18th century when Lord Cavendish of England determined the mass of the Earth[2], and hence established the density of the bulk Earth to be approximately 5.45 g/cm^3 (the presently accepted bulk Earth density is 5.25 g/cm^3). The implications of these calculations were far-reaching. Most of the rocks on the Earth's surface have densities between 2.5 and 3 g/cm^3, and thus somewhere in the Earth's interior must contain a denser component. These calculations have been further verified and refined by seismological studies and studies of the Earth's moment of inertia. In particular, in 1906, Richard Oldham of the Geological Survey of India, used seismic waves (elastic waves in the Earth's interior created by earthquakes) to show that the Earth was largely partitioned into two major reservoirs: the central core, with a radius of ~0.4 that of the Earth's radius, and the surrounding mantle. The boundary between the core and the mantle was found to coincide with a distinct density and seismic velocity jump (Fig. 2.1), confirming earlier suggestions of an Earth with a dense interior.

The combination of gravity, inertia, and seismic measurements constrained the Earth's core to have a density of ~10 g/cm^3, but density alone cannot provide unequivocal information on what the core is made of as many materials have the same density. For example, heavy metals such as silver, iron, nickel, copper, tin, molybdenum, cadmium, ruthenium, and palladium, all have densities within the range of 7 to 13 g/cm^3. In 1961, Francis Birch of Harvard University constructed an elegant experiment that resolved this amibiguity. He empirically determined how a material's seismic velocity, density, temperature and chemical composition are related (Fig. 2.2). Importantly, he showed that not only were solids more compressible than believed at that time, but most materials have an unique density-seismic velocity relationship associated with compression. In fact, at the very high pressures characteristic of core conditions, Birch not only showed that the density of iron metal increased to ~10 g/cm^3 compared to 7.9 g/cm^3 at atmospheric pressures, but also showed that the velocity-density relationship of iron metal fit very closely that inferred from seismic studies. The combination of experimental mineral physics and seismology established that the core must be predominantly made up of compressed Fe, whereas the mantle is made up primarily of silicates[3].

[2] In 1798, Cavendish determined the gravitational constant using a torsion balance. He then used this number in a pendulum experiment and was able to determine the mass of the Earth from the period of the swinging pendulum. Even earlier, however, Pierre Bourguer of France had visited the Andes in 1748 in order to study the Earth's magnetic field. Instead, Bourguer made the interesting observation that his plumb line was deflected from vertical towards the Andes. The English astronomer Nevil Maskelyne used this observation to determine the mass of the Earth, yielding a density of 4.5 g/cm^3.

[3] In detail, the velocity-density relationship of Fe metal does not fit exactly that inferred from seismic studies of the core: seismic studies predict a slightly lower density than pure Fe (Fig. 2.2). It appears that although the core must be made up predominantly of Fe (and Ni), there must be a small proportion of a light element in the core in order to explain its slightly lower density. Elements, such as O, S, Si, and K, have all be suggested, but there is presently no consensus.

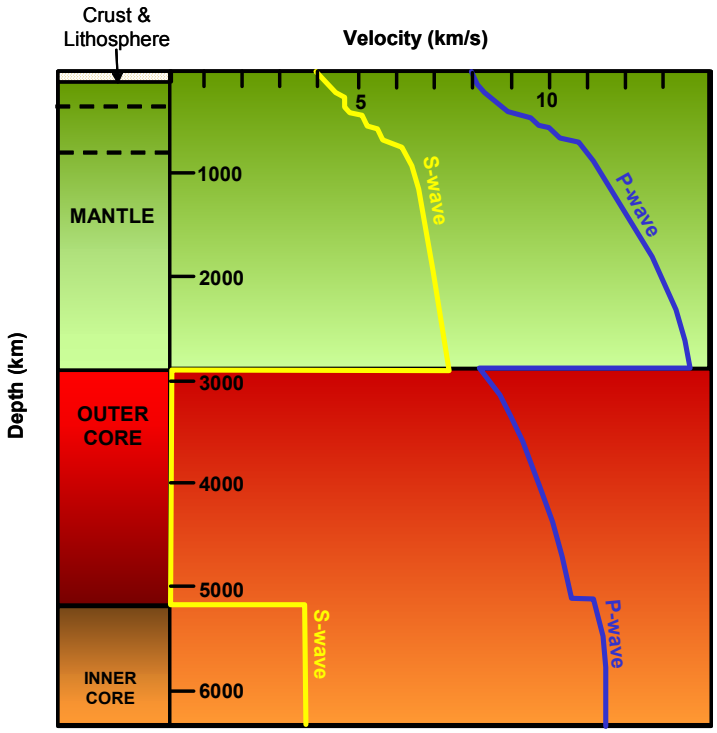

Figure 2.1. Seismic velocity structure of the Earth. P-wave and S-wave refer to compressional and shear wave velocities. S-waves do not propagate through liquid, hence go to zero in the outer core. Dashed lines represent the 410 and 660 km discontinuities in the mantle; they are associated with phase changes rather than

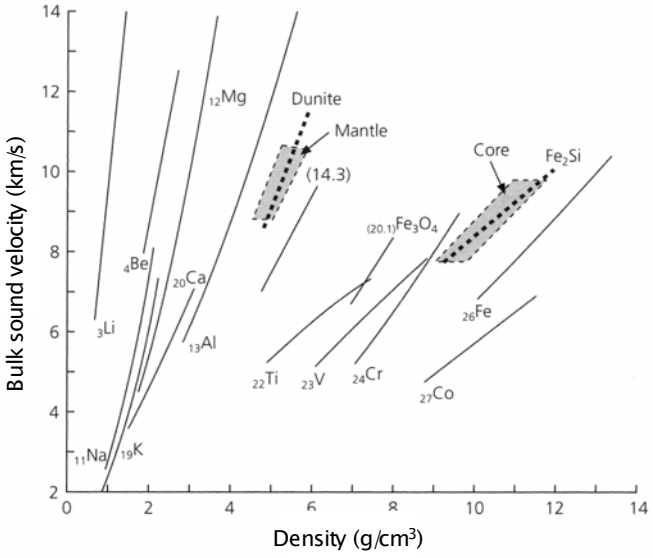

Figure 2.2. Francis Birch's [*Birch*, 1968] velocity-density experiments for various metals and silicates (dunite). Hatched zones represent observed bulk soundwave velocity-density relationships in the mantle and in the core. It can be seen that the core velocity-density relationships more closely fit that of metallic Fe than silicates.

The question we are left with is how and when was Earth's radial heterogeneity established? One possibility is that this radial heterogeneity is primordial, that is the Earth was layered from the outset: Karl Turekian and Sydney Clark of Yale University suggested that the solid particles making up the Earth were assembled in order of decreasing density, or in other words, "heterogeneously accreted" (Fig. 2.3). In this hypothesis, iron, being very dense, accreted first to form the core, while silicates, being less dense, accreted afterwards, forming the mantle. An opposing hypothesis is that the Earth was "homogeneously accreted" (Fig. 2.3), that is, the Earth was initially a homogeneous mixture of metallic Fe and silicates, the formation of the metallic core being the result of metal-silicate segregation after most of the Earth had been accreted. It is now believed that the latter is most likely but that core-mantle segregation occurred very shortly after the Earth accreted.

2.1.2 Constraining the bulk Earth composition

Returning to our task of calculating the composition of the bulk Earth, common sense dictates that the most straightforward way is to combine the major reservoirs in the Earth (Fig. 2.4). This approach, of course, requires that we know the number, mass and composition of each of these reservoirs. How do we know how many reservoirs there are and how big they are? And even if we knew this information, how do we even know that these reservoirs are homogeneous? Unfortunately, it is impossible to answer all these questions. We are thus forced to make assumptions, which means that whatever estimate we make is model-dependent and the uncertainties come down to how good we think our assumptions are.

When making models, the best approach is to start simple, building the complexity progressively. Thus, let us first assume that the "solid" Earth can be roughly subdivided into a metallic core and a silicate mantle. In so doing, we implicitly assume for simplicity that all

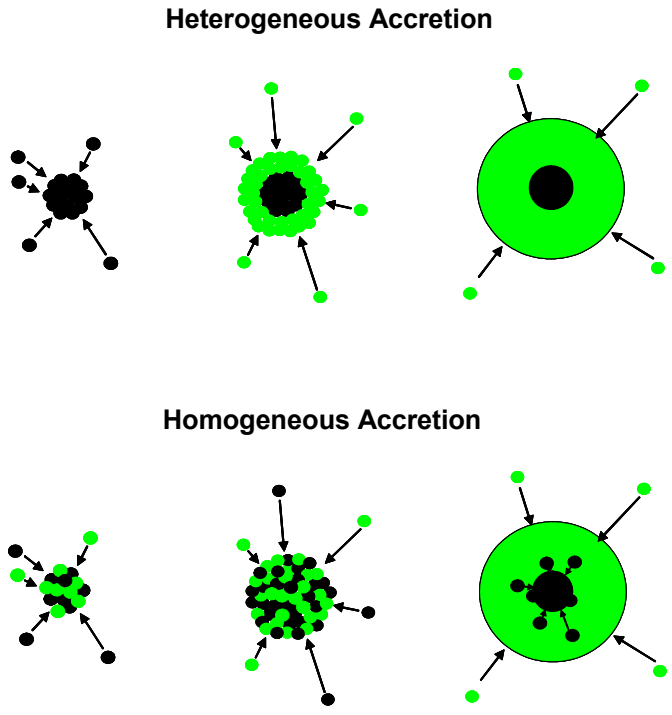

Figure 2.3. Schematic diagram showing two different scenarios for the formation of the Earth (modified from C. J. Allegre, "From Stone to Star", 1992)

crustal reservoirs are included in this silicate mantle, hence we will refer to this silicate component as the bulk silicate Earth (BSE). You might consider the bulk silicate Earth to represent the primordial mantle just after core segregation but before extraction of crust (remember, this is a model!). Experimental data indicate that some elements (e.g., the alkalis, Ca, Mg, Al, and the rare-earth elements) prefer to be in silicates rather than alloyed with metal; such elements are called ***lithophile*** (*litho*=rock; *phile*=love) and are not present in the core. Thus, the concentration of any lithophile element in the bulk Earth is simply given by the weight fraction of the bulk silicate Earth (62.5 %) multiplied by its concentration in the bulk silicate Earth. Those elements that prefer to alloy strongly with Fe metal, such as Pt, Pd, Ir, Os, Ru, Au, and Ni, are called ***siderophile*** elements (*sidero*=iron). In a similar way, their concentrations in the bulk Earth can be determined by assuming their concentrations in the bulk silicate Earth are very small in comparison to the metallic core.

The problem, however, is that we do not know from the outset the composition of the bulk silicate Earth nor do we know the concentration of siderophile elements in the Fe core. To complicate matters further, the bulk silicate Earth has differentiated into many reservoirs, e.g. the continental crust, oceanic crust, and that part of the mantle that is residual to the extraction of crust (the "depleted mantle"); thus, it may be difficult to find a relict sample of the bulk silicate Earth. Adding up these derivative silicate reservoirs is not a trivial task as a number of uncertainties can arise. The composition of each reservoir may be uncertain due to either the lack of samples or to heterogeneity within a reservoir (e.g., the continental crust is highly heterogeneous vertically and laterally). The precise amount of continental or oceanic crust that has been hidden somewhere (e.g., not re-mixed) in the mantle is also not known well. In addition, it must be assumed that the presence of other reservoirs has not been overlooked. Finally, the size of the depleted mantle and that of any undifferentiated parts of the mantle is not known. Thus, estimating the bulk silicate Earth composition by a mass balance approach will

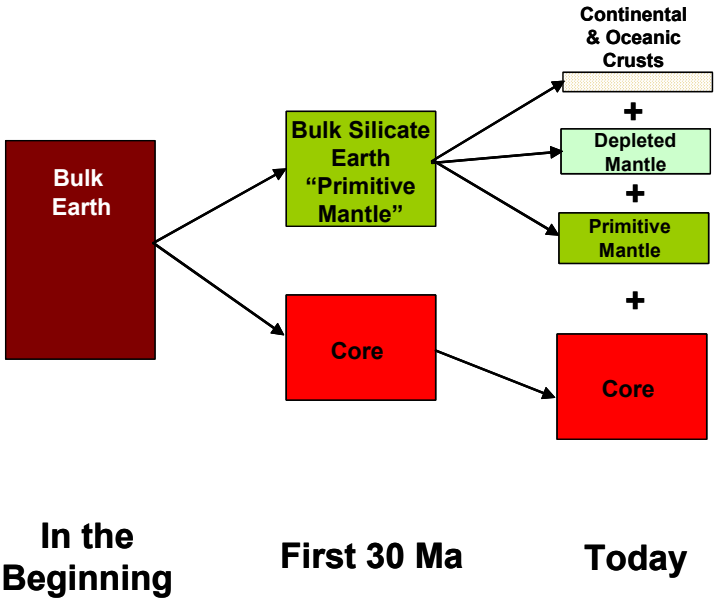

Figure 2.4. Schematic diagram illustrating the simple approach for determining a model bulk composition of the Earth by adding up all the hypothesized reservoirs that have formed.

require a number of assumptions. It sounds like our model of the bulk Earth is itself going to be built on a model of the bulk silicate Earth!

It may not, however, be so bad. In the following subsections, we will discuss different ways of constructing the composition of the bulk silicate Earth (we will discuss the composition of the core later). We will use the term, "primitive mantle", to describe any parts of the mantle (which may no longer exist) that have somehow escaped differentiation (e.g., melt extraction) and therefore, retain their original composition from the time of Earth's formation. Defined in this way, the composition of a sample of "primitive mantle" should be equal to the composition of the bulk silicate Earth insofar as the primitive mantle was not compositionally stratified (this

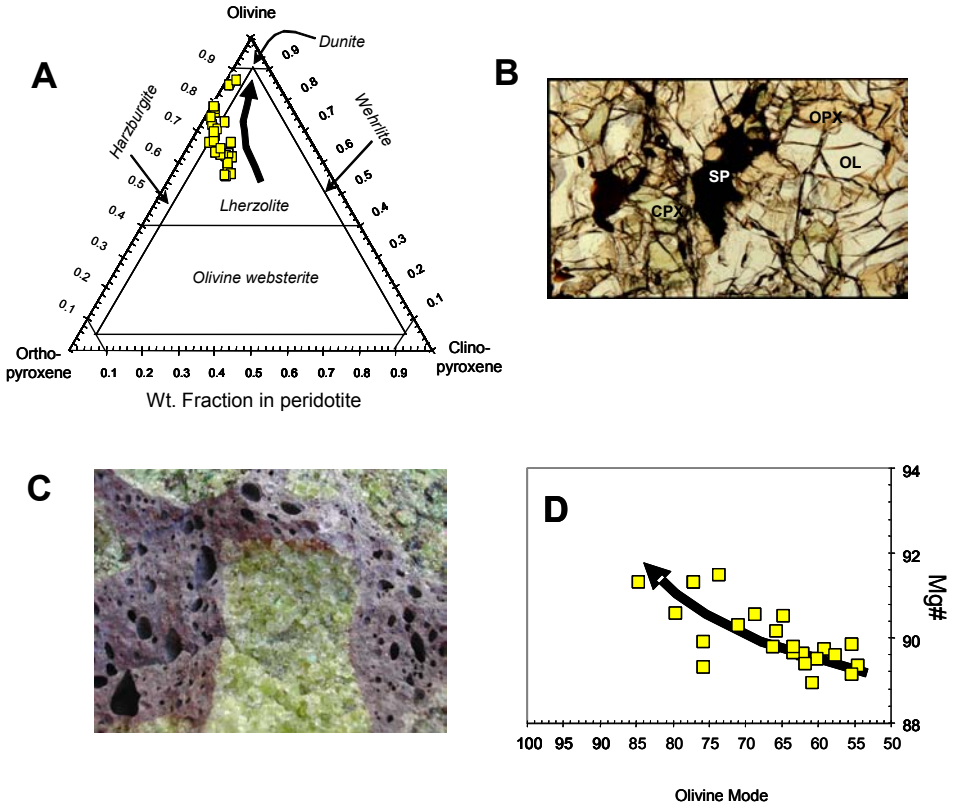

Figure 2.5. Peridotites are olivine-rich rocks containing variable amounts of orthopyroxene, clinopyroxene, and an aluminous phase (plagioclase, spinel or garnet). The type of aluminous phase depends primarily on pressure. For primitive peridotites (e.g., those that have experienced very little melt extraction), the spinel transitions to garnet after pressure is increased beyond ~1.5 GPa (or ~45 km). Figure 2.5a shows the observed range in peridotite mineralogy in olivine-orthopyroxene-clinopyroxene wt. % space normalized to the aluminous phase; the arrow represents the direction of progressive melt extraction. Figure 2.5b and c show how a peridotite xenolith looks under thin section and in hand-sample. Figure 2.5d shows how Mg# (100×molar Mg/(Mg+Fe)) and olivine mode of Phanerozoic peridotites varies as melt is progressively extracted (arrow). Primitive peridotites, i.e. those that have experienced minor amounts of melt extraction, are characterized by Mg#'s of ~89, and significant amounts of clinopyroxene and orthopyroxene in addition to olivine; such peridotites are classified as lherzolites. With increasing

is still a very active topic of debate). We thus seek to determine the composition of the Earth's primitive mantle.

2.1.3 Constraining the composition of the bulk silicate Earth – the primitive mantle

We know that the continental crust and oceanic crust represent the solidified products of magmas generated by partial melting of the mantle. In the case of oceanic crust, we will learn later that its composition is classified as basaltic, a melt composition that is derived directly from partial melting of the mantle. The continental crust, on the other hand, has dioritic or andesitic compositions, which we will later learn represent the end-products of the compositional evolution of the magma during emplacement and cooling, and therefore, do not represent direct melts of the mantle[4]. Progressive extraction of oceanic and continental crust from the mantle should leave behind a residual mantle, whose composition is modified due to the loss of meltable components (e.g., Ca and Al). The rate and style at which the residual mantle evolves from its primitive composition at the beginning of Earth's history depends not only on the rates and composition of crust generation, but also on the rates at which crust is returned and re-homogenized into the mantle. As much of the mantle has probably been processed through the crust-making factory, we must either hope to find a relict piece of primitive mantle or infer its composition.

Searching for a relict sample of primitive mantle

By the late 1950's, there was increasing evidence that the mantle was made up of peridotite (Figure 2.5), an Mg-rich rock (molar Mg/(Mg+Fe) = Mg# ~ 0.89-0.93) consisting of pyroxene, olivine and an aluminous mineral phase (plagioclase, garnet, or spinel)[5]. This evidence came directly from studies of peridotite xenoliths entrained in basaltic lavas, the xenoliths representing fragments of wall-rock ripped up from the source regions of the host lavas. In 1964, David Green presented a study of a large exposure of peridotite in Cornwall, England, called the Lizard peridotite massif [*Green*, 1964a; *Green*, 1964b; *Green*, 1964c]. He found evidence for the reaction of spinel and aluminous pyroxene to form plagioclase, the direction of this reaction indicating a decrease in pressure. Green suggested that this peridotite outcrop was once part of a mantle diapir that initially rose from high pressures and was ultimately emplaced at shallow crustal pressures, perhaps in a rift or back-arc.

The collective evidence from these mantle samples indicates that peridotites have a range in composition, extending from a very fertile endmember characterized by a high concentration of meltable components (e.g., Ca, Al, K, P, and Na) to a depleted endmember with low concentrations of meltable components (Fig. 2.6). The former, called lherzolites, are characterized by Mg#'s between 0.88-0.90, 3-4 wt. % CaO and Al_2O_3, and the presence of clinopyroxene. The latter, called harzburgites, are characterized by Mg#'s between 0.90-0.93, <3 wt. % CaO and Al_2O_3, and the lack of clinopyroxene. If meltable components are severely depleted, then the peridotite consists almost entirely of olivine and is termed a dunite.

---

[4] While it is obvious that we could never use continental crust to infer the composition of the mantle due to the multi-step nature of continental crust formation, one might wonder whether basalts, which are direct melts of the mantle, provide a viable solution. Unfortunately, life is rarely so simple. It is likely that even basalts have experienced some degree of chemical evolution during their emplacement. In addition, as we will learn later, the Si composition of basalts is typically buffered (e.g., maintained at a constant concentration) over a wide range in residual compositions because of the SiO_2-buffering assemblage of orthopyroxene and olivine.

[5] The mineralogy of these peridotite xenoliths was first documented in Ross, C.S., M.D. Foster, and A.T. Myers, Origin of dunites and olivine-rich invlusions in basaltic rocks, *Am. Mineral.*, *39*, 693-737, 1954.

This spectrum of compositions is believed to reflect the effects of extracting variable amounts of basaltic melt. Thus, one approach at estimating the primitive mantle composition is to assume that the least depleted end of the compositional spectrum represents the primitive mantle, e.g., that part of the mantle that has experienced no melt extraction. The most primitive peridotites appear to have Mg#'s between 0.89-0.90 and 3-4 wt. % CaO and Al_2O_3. By taking the average of the most primitive mantle peridotites collected from the field, Emil Jagoutz and co-workers [*Jagoutz et al.*, 1979] derived a model major-element composition for the primitive mantle (Table 2.1).

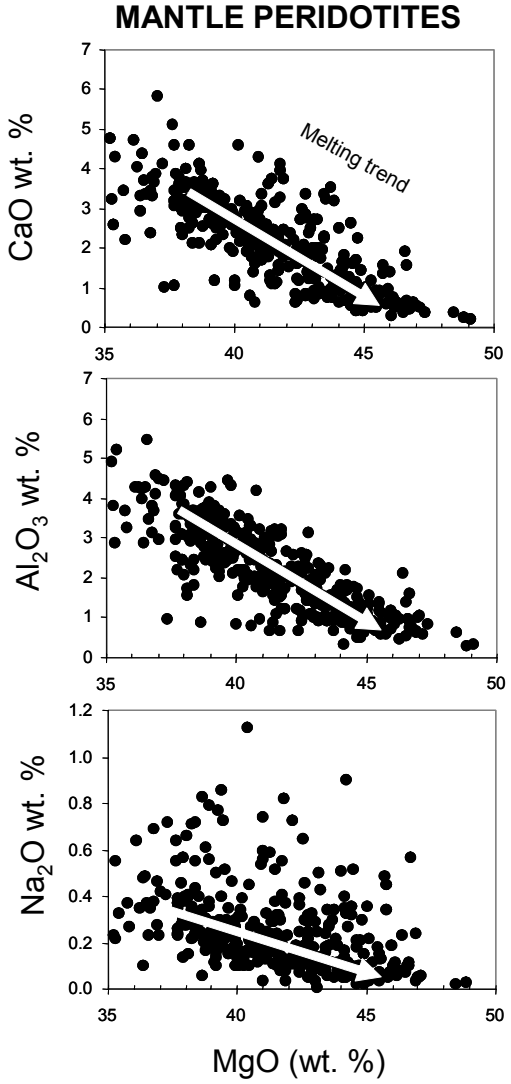

Figure 2.6. Compositional variations exhibited by mantle peridotites. White arrows represent the direction of increasing melt extraction. Some of the scatter, particularly, in Na_2O is due to the secondary effects of melt or fluid infiltration.

Text Box 2.1. The Pyrolite Concept

A term that often comes up in the petrologic literature is "pyrolite". Pyrolite is a model primitive mantle composition created by Ted Ringwood from Australia in 1962. Together with fellow Australian David Green, Ringwood recognized the fact that the mantle was largely made up of pyroxene and olivine (hence the name pyrolite) and attempted to derive a model composition for the source of mid-ocean ridge basalts. They assumed that the primitive mantle had an Mg# of 89-90 and 3-4 wt. % CaO and Al_2O_3 on the basis of the least depleted peridotite observed. In order to reconstruct the remaining major- and minor-element compositions, they reasoned that one could simply recombine a mantle-derived melt (e.g., basalt) with a melt-depleted peridotite (e.g., harzburgite or dunite) in proportions such that the final mixture would be constrained to have an Mg# of 0.89-0.90 and 3-4 wt. % CaO and Al_2O_3. The concentration of other elements would then be dictated by their concentrations in the two mixing endmembers and by the mixing proportion. In this manner, the first pyrolite model came to be a combination of a primitive basalt (Mg# ~ 73) with a dunite in proportions of 1:3. Since then, other pyrolite model compositions have been introduced. All pyrolite models are based on the same concept.

Table 2.1. Different models for the major-element composition of the bulk silicate Earth (primitive Mantle)

	1	*2*	*3*	*4*	*5*	*6*	*7*	*8*
MgO	38.1	38.1	38.3	36.8	35.5	37.8	37.8	36.3
Al_2O_3	4.6	3.3	4.0	4.1	4.8	4.1	4.4	4.7
SiO_2	45.1	45.1	45.1	45.6	46.2	46	45	45.6
CaO	3.1	3.1	3.5	3.5	4.4	3.2	3.5	3.8
FeO	7.9	8	7.8	7.5	7.7	7.5	8.1	8.2
Total	98.8	97.6	98.7	97.5	98.6	98.6	98.8	98.5
Mg#	0.896	0.895	0.897	0.897	0.891	0.899	0.893	0.888

Mg# = Mg/(Mg+Fe)

1. [*Ringwood*, 1975]
2. [*Ringwood*, 1979]
3. [*Jagoutz et al.*, 1979]
4. [*Wänke et al.*, 1984]
5. [*Palme and Nickel*, 1985]
6. [*Hart and Zindler*, 1986]
7. [*O'Neill and Palme*, 1998]

It is now worth pausing to note that using the least depleted peridotite to estimate primitive mantle, strictly speaking, yields only a minimum estimate of the concentration of meltable components in primitive mantle because a significant amount of the present mantle has already been processed to form the continental crust. In the case of major-elements, the uncertainty introduced into Jagoutz's primitive mantle model is very small because the

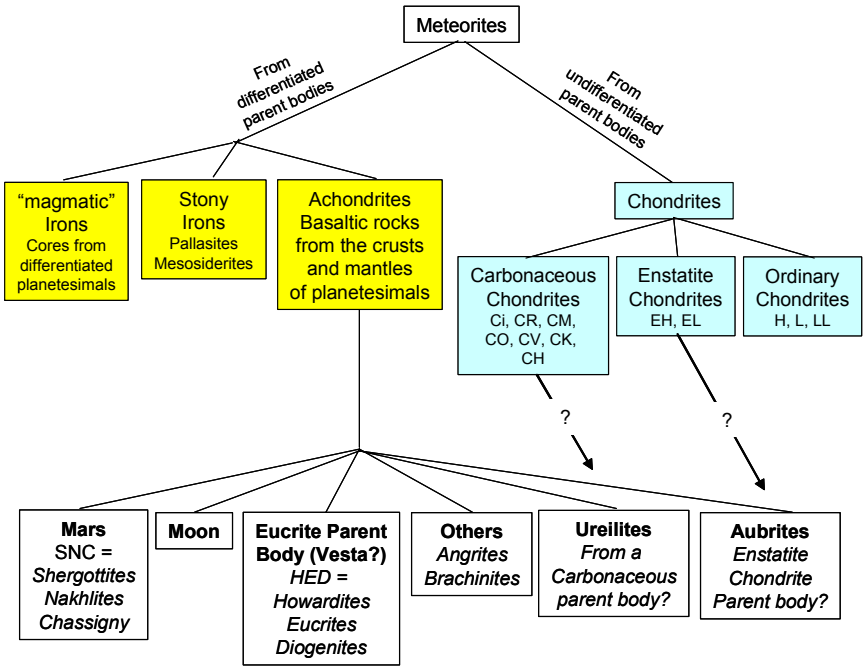

Figure 2.7. Meteorite classification diagram (borrowed from [*O'Neill and Palme*, 1998]).

continental crust makes up only 0.38 % of the mass of the bulk silicate Earth hence, extracting continental crust from the mantle does not noticeably affect the major-element signature of the residual mantle. By contrast, many of the highly incompatible trace-elements (e.g, Cs, Ba, Rb, Sr, and U) are so enriched in the continental crust (anywhere from 30 to 90% of the bulk silicate Earth's total budget of these elements may be housed in the continental crust) that even the most fertile peridotite samples appear to be slightly depleted in these elements. Thus, in order to constrain the trace-element composition of the primitive mantle, Jagoutz and his co-workers turned to meteorites for help. We will discuss the meteorite perspective in the next section.

Inferring the primitive mantle composition from undifferentiated meteorites

As discussed in the previous section, looking at the least differentiated peridotites provides a good estimate of the major-element composition of the bulk silicate Earth, but it may not provide a good estimate of the trace-element composition. An independent means of estimating both the major and trace-element composition of the bulk silicate Earth is to turn to undifferentiated meteorites. Approximately 82% of all meteorite falls represent undifferentiated meteorites, which are meteorites that do not show any evidence of having been melted since the formation of their parent bodies when the solar system formed (4.55 Ga). The remaining meteorite falls are differentiated meteorites, which represent fragments of parent bodies that have differentiated into cores, mantles and crusts. Figure 2.7 shows a current classification scheme for meteorites. The undifferentiated meteorites are called ***chondrites***, a name given to describe the unique texture of spherical to ellipsoidal structures in all but one of the chondrite meteorite groups. Mineralogically, chondrites are composed of mixture of silicate minerals (pyroxene and olivine) and Fe-Ni metal grains. If we were able to extract these metal grains from some types of chondrites, for example by using a magnet, we would find that the remaining silicate proportion

Text Box 2.2. Classification of chondrites

Chondrites can be divided into three clans based on their major-element compositions and the ratio of Fe bounded to metal and sulfides to Fe bounded as oxides in silicates. The latter is a function of the oxygen fugacity of the meteorite. In high oxygen fugacity environments, the Fe is bound up in silicates as Fe^{2+}, whereas in low oxygen environments, the Fe is bound in metals as Fe^{0}. Figures 2.9 and 2.10 show how these clans can be distinguished from each other.

With this classification, the three chondrite clans are: enstatite, ordinary, and carbonaceous chondrites. Enstatite chondrites contain the lowest Mg/Si ratio and also appear to be the most reduced. Carbonaceous chondrites have the highest Mg/Si and appear to be the most oxidized. Ordinary chondrites appear to be intermediate in Mg/Si and in oxidation state. The names chosen for these meteorite clans derive from historical classifications based on mineralogy. Enstatite chondrites are named for their high abundances of enstatite. Ordinary chondrites are named because they are the most abundant clan. Carbonaceous chondrites all have carbon although they were mistakenly named because it was thought they all had higher carbon contents than other chondrites.

Each chondrite clan can be subdivided even further based on their petrologic characteristics. Figure 2.11 shows all the groups that arise. Letters are given for each chondrite group, and numbers are given to denote the degree of thermal metamorphism on a scale of 1 to 6. Also included in Figure 2.11 are Rumuruti and Kakangari meteorites; both are new clans of meteorites represented by only one meteorite fall each and are therefore extremely rare.

The most obvious feature of Figure 2.11 is that carbonaceous chondrites have experienced the least amount of thermal metamorphism, whereas ordinary and enstatite chondrites have experienced moderate to high degrees of thermal metamorphism. As described in the main text, this petrologic classification scheme agrees well with the elemental composition of these meteorites. CI carbonaceous chondrites, classified as petrologic type 1, are characterized by a fine-grained matrix and high carbon and water contents, which collectively indicate that CI chondrites have retained much of their volatile elements because they were not thermally metamorphosed. Except for the most volatile elements, recall that CI carbonaceous chondrites have solar elemental abundances. All other chondrites, having experienced variable degrees of thermal metamorphism, have lower volatile element abundances relative to CI proportions.

has a bulk composition similar to that of mantle peridotites on Earth[6]. These characteristics collectively suggest that we may be able to shed light on the composition of the bulk silicate Earth by studying chondritic meteorites. As we will discover below, such meteorites essentially retain their bulk compositions from the birth of the solar system and provide our best view into what the primitive Earth may have looked like.

[6] This analogy was borrowed from Allegre, C.J., *From stone to star: a view of modern geology*, 287 pp., Harvard University Press, Cambridge, 1992. The author of this book shared a Crafoord Prize in 1986 with Gerald J. Wasserburg of Caltech for their pioneering studies of isotope geochemistry.

Before continuing our task of reconstructing the Earth's primitive mantle composition, we need to review some of the salient features of chondritic meteorites. One of the striking features of chondrites is that their elemental compositions are very similar to that of the sun (except for the gaseous elements, most of which are not retained in meteorites), the latter as determined by spectroscopic measurements of the solar photosphere. The most primitive group of chondrites, the CI *carbonaceous chondrites*, has relative elemental abundances nearly identical to that of the solar photosphere (a description of the other chondrite groups is given in the Text Box 2.2). Figure 2.8 shows solar elemental abundances versus CI carbonaceous chondrite abundances expressed as the number of atoms per 10^6 Si atoms. Elemental

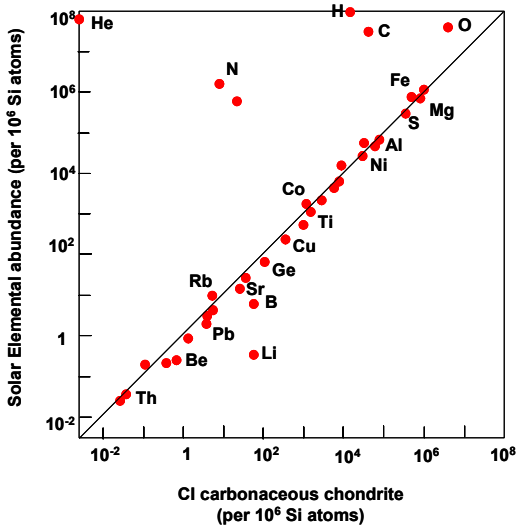

Figure 2.8. Elemental abundances (normalized to 10^6 Si atoms) of CI carbonaceous chondrites versus the solar photosphere.

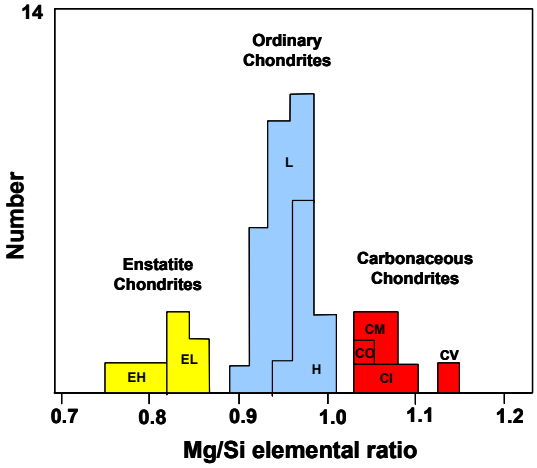

Figure 2.9. Elemental Mg/Si ratio histogram of chondritic meteorites (adapted from Figure 5.3 in [*Norton*, 2002]).

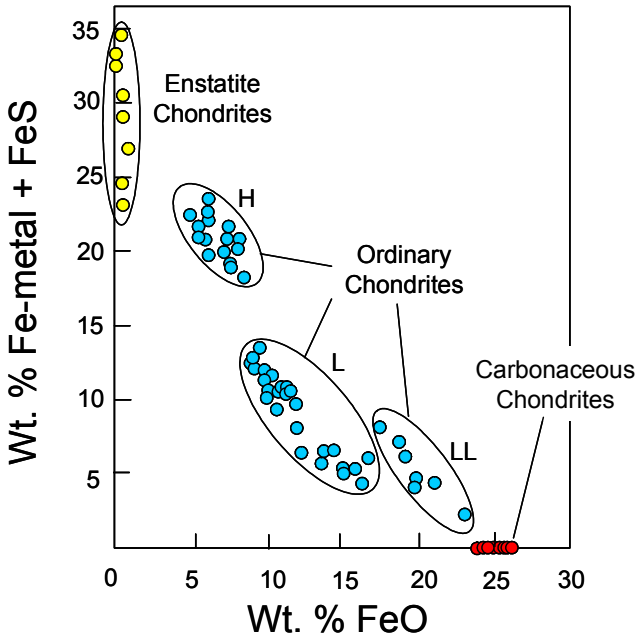

Figure 2.10. Ratio of metal- and sulfide-bound Fe to silicate-bound Fe (expressed as FeO). Figure is borrowed from Figure 5.4 in [*Norton*, 2002].

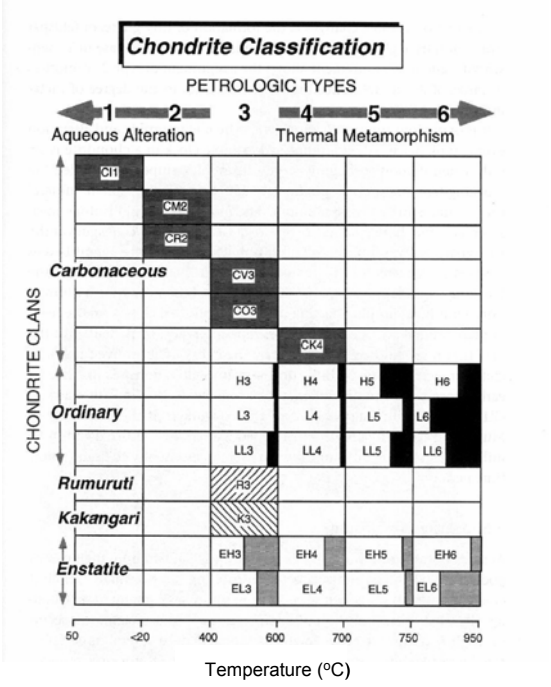

Figure 2.11. The meteorites clans can be further subdivided according to their petrologic textures and compositions. Numbers between 1 to 6 are given to reflect increasing degrees of thermal metamorphism. Letters are given to denote each meteorite group. Figure taken directly from Figure 2.13 in [*McSween*, 1999]. The shaded areas in each box reflect the relative proportions of the various petrologic types for each chondrite group.

abundances have been normalized to Si because it is difficult to determine absolute abundances in the solar photosphere. As the sun accounts for 99 % of the mass of the total solar system, the composition of the sun must closely match that of the solar nebula before it condensed and differentiated to form the sun and the surrounding planets. The solar composition of CI carbonaceous chondrites underscores the primitive nature of this meteorite group.

Another distinctive feature of chondrites is their high degree of heterogeneity. The chondrules that occur in all but one of the chondrite groups show textural features, which indicate they are the products of rapid cooling of numerous ferromagnesian silicate melt droplets. The matrix that binds the chondrules consists of a disequilibrium mixture of minerals ranging from those formed at very high temperatures (>1400 K) to very low temperatures (~273 K). Although chondrites have experienced variable degrees of reheating, the preservation of this disequilibrium assemblage of high temperature and low temperature minerals attests to the primitive nature of these meteorites.

These observations led to the *condensation model* for the birth of the solar system. John Larimer and Ed Anders of the University of Chicago [*Larimer and Anders*, 1967] along with Larry Grossman [*Grossman*, 1972] proposed that the solar system formed as a result of cooling of a hot and more or less homogeneous gaseous nebula. As the nebula cooled off, certain chemical compounds became unstable, precipitating (*condensing*) directly as solids rather than liquids due to the very low pressures in the solar nebula. At first, small dust grains were created. These dust grains then accreted to each other, forming the parent-bodies of meteorites and ultimately the planets (the liquid droplets represented by the chondrule textures were formed by a flash-heating process that occurred during the condensation of the solar nebula).

In particular, Grossman was able to calculate the sequence of mineral condensation reactions from a cooling solar nebula by making chemical equilibria calculations. He showed that the first minerals to condense are Ca-Al-rich inclusions (CAIs), which are Ca-, Al-, and/or Ti-oxides that condense at >1400 K. The next minerals to condense are the Fe and Ni metal alloys at ~1300 K, followed by ferromagnesian silicates at ~1100 K. Feldspars and sulfides condense between ~800-1100 K, and finally at much lower temperatures, those compounds containing volatile elements, such as hydrous silicates and water, condense. A schematic diagram of this condensation sequence is shown in Figure 2.12. The cooling of the solar nebula and accretion of these condensed particles is believed to have occurred within 5 to 10 Ma after the formation of the CAIs, the initial solar condensates.

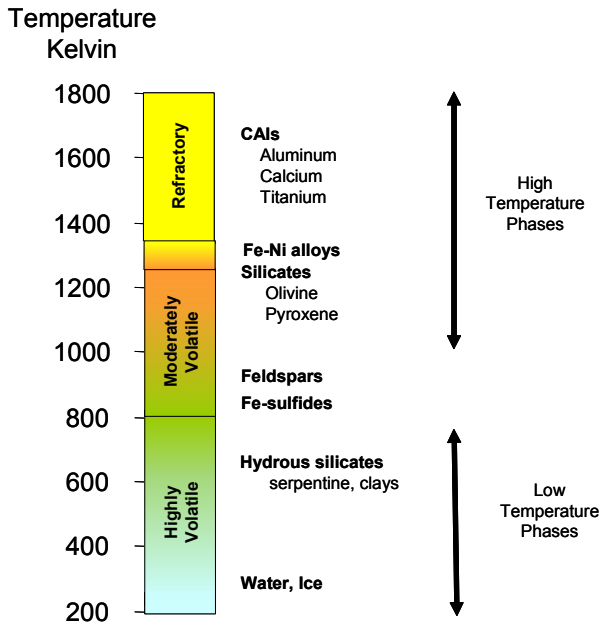

Figure 2.12. Sequence of condensation reactions from a cooling solar nebula. Simplified from [*Grossman*, 1972]. .

In making these chemical equilibria calculations, Grossman was also able to determine the temperatures at which particular elements condensed to the solid

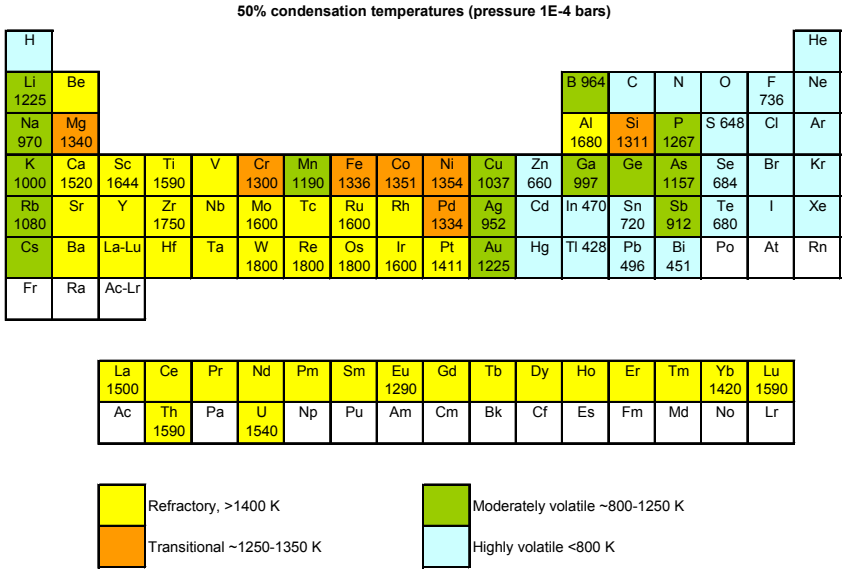

Figure 2.13. 50% condensation temperatures taken from [*Wasson*, 1985] and [*O'Neill and Palme*, 1998].

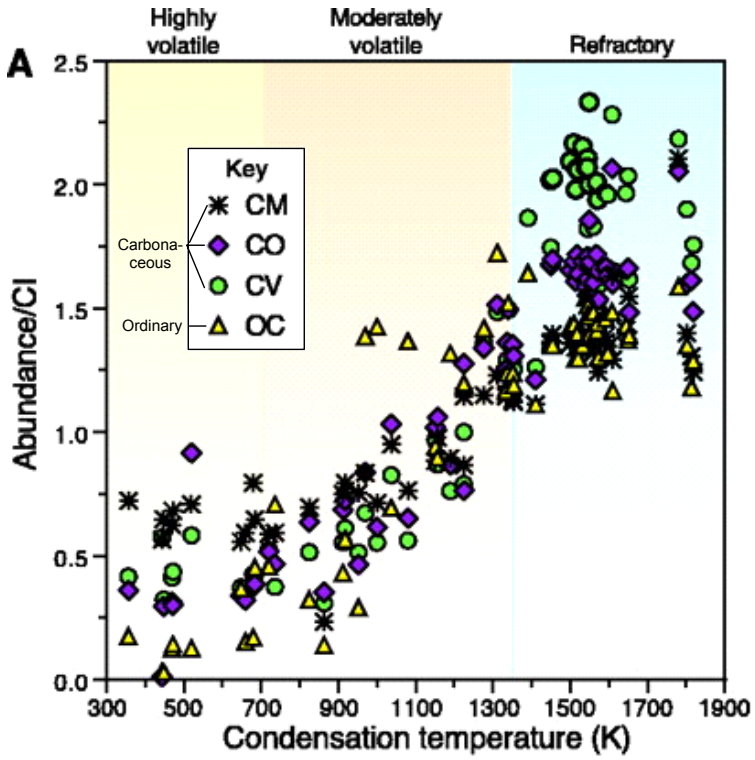

Figure 2.14. The CI chondrite normalized elemental abundances in bulk carbonaceous (CM, CO, and CV) and ordinary chondrites (OC) versus their 50% condensation temperatures. The correlation between abundance and condensation temperature (volatility) is striking. The elements are divided into refractory (>1350 K), moderately volatile (700 to 1350 K), and highly volatile (<700 K). The common elements (Mg, Si, and Fe) have been included with the moderately volatile elements to simplify the plot. The three ordinary chondrite groups have been combined, also to simplify the plot. Figure and figure caption taken directly from [*Alexander et al.*, 2001].

phase. Some elements, such as Ca, Al, Ti and the rare earth elements (REEs), condense as oxides at very high temperatures (>1400 K). These elements are referred to as *refractory*, a cosmochemical term used to describe their high temperature associations. Elements, such as Mg, Si, and Fe, also condense at high temperatures, but at temperatures slightly below that of CAI condensation because most of these elements condense out with the silicate minerals (1250-1350 K). Elements, such as O, N, C and the noble gases, not surprisingly, have a tendency to form gaseous compounds; these elements condense out of the solar nebular only at very low temperatures (<800 K) and are hence termed *volatile*. Elements, such as Ga, Ge, As, Na, K, Rb, and Cs, which condense at intermediate temperatures (800-1250 K) are termed moderately volatile. Figure 2.13 shows how all the elements are classified according to the temperature at which 50% of their total abundance in the solar nebular has condensed.

An important feature of this condensation sequence is that it is very difficult to fractionate refractory element abundance ratios during condensation because of the narrow temperature range over which the minerals harboring these elements condense. By contrast, the mineral phases harboring the volatile elements condense over a wide temperature range, and thus, volatile element abundances are more readily fractionated. This feature is seen if we examine the elemental abundance patterns of the various chondrite groups in detail. In Figure 2.14, the elemental abundances of several chondrite groups normalized to CI carbonaceous chondrite are plotted in the order of increasing condensation temperature. Recall that the CI carbonaceous chondrite group has solar elemental abundances minus the highly volatile elements, C, N, and O[7]. Deviations from the CI carbonaceous chondrite's elemental abundance pattern indicates that some sort of elemental fractionation has occurred. It can be seen from Figure 2.14 that for a given chondrite group, the refractory elements are present in solar proportions, regardless of their absolute abundances. In contrast, the moderately volatile elements for all chondrite groups, except for CI carbonaceous chondrites, appear to be highly fractionated as evidenced by the sloping abundance pattern. In summary, chondrites have solar relative proportions of the refractory elements, but not necessarily solar proportions of the moderately volatile and highly volatile elements.

We can now use this information to make inferences about the composition of the bulk silicate Earth. Assuming that the primitive Earth formed from undifferentiated rocky planetesimals, it follows that the bulk Earth should have chondritic or solar relative abundances of the refractory elements. For those refractory elements that do not enter the core but instead reside in the silicate mantle (*refractory lithophile elements*), it also follows that the bulk silicate Earth, or primitive mantle, possesses chondritic relative abundances.

The foregoing, however, only permits us to determine the ratios of refractory lithophile elements in the Earth's primitive mantle. It does not allow us to determine the absolute abundance of any element. This is apparent as follows. In Figure 2.15, we plot various meteorite groups and terrestrial rocks in terms of Mg/Si versus Al/Si. Al is a refractory element, while Mg and Si are in the transition between refractory and moderately volatile. Figure 2.15 shows that Mg decreases with increasing Al in terrestrial rocks, while Mg increases with increasing Al in the meteorite groups. Importantly, we see that the major element compositions of terrestrial rocks are not matched by any chondrite groups. Thus, while it is valid to assume that the Earth's refractory lithophile elements are in chondritic proportions, the fact that the major element composition of the bulk Earth is not matched by any meteorite group indicates that not only can

[7] By convention, the elemental abundance pattern of CI carbonaceous chondrites is used to represent solar relative abundances (except for the highly volatile elements) because the geochemical data on meteorites is of much higher precision and accuracy than that on the solar photosphere.

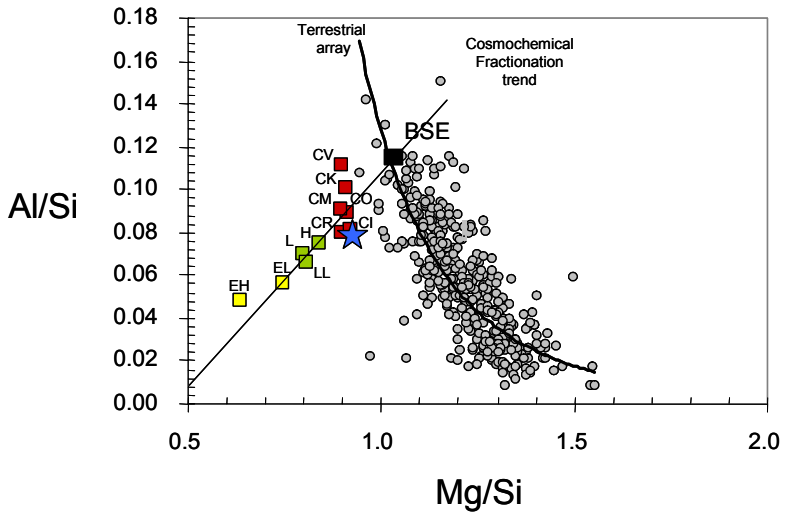

Figure 2.15. Elemental Al/Si and Mg/Si of various chondrite groups (see Text Box 2.2 for classification scheme) and spinel-peridotite xenoliths from the Earth's mantle (gray circles). Black square labeled BSE is an estimate of the bulk-silicate Earth. Unlabeled blue star represents the solar photosphere value. Curved line represents a quadratic regression through the mantle peridotite data (**the terrestrial array**). Straight line represents the cosmochemical fractionation line of [*Jagoutz et al.*, 1979], which is regressed through the chondrite data.

we not obtain direct information on absolute elemental abundances in the Earth from meteorites, but we also cannot obtain the relative abundances of moderately volatile and volatile elements in the Earth by direct comparison to meteorites.

A clever solution to this problem was presented by Jagoutz et al. [1979]. They suggested that the intersection between the terrestrial array and the chondrite array might represent the Mg/Si and Al/Si of the Earth's primitive mantle. That this intersection approximately matches the composition of the most fertile mantle peridotites (as well as various pyrolite models – see Text Box 2.1) suggests that the bulk silicate Earth indeed has a major-element composition different from chondritic meteorites[8]. Importantly, they recognized that some of these primitive mantle samples have chondritic refractory element ratios (e.g., chondritic Ca/Al and Ti/Al ratios). Those that have been depleted in meltable components have non-chondritic refractory element ratios due to the different behaviors of these elements during melting. They thus reasoned that one could determine absolute elemental abundances by extrapolating compositional trends in melt-depleted peridotites back to where refractory element ratios become chondritic. Once the absolute abundance of one element has been determined by such an extrapolation, the abundances of other elements follow from their ratios to each other. This approach forms the basis for nearly all subsequent models proposed for the composition of the primitive mantle. Some elements are exceptions in that their primitive mantle abundances are determined by other approaches, such as isotopic constraints (e.g., the primitive mantle Rb/Sr ratio is extrapolated from correlations between Sr and Nd isotopes). Table 2.3 shows a recent comprehensive model for the primitive mantle taken from [*McDonough and Sun*, 1995].

[8] The higher Mg/Si ratio of the bulk silicate Earth has been interpreted as indicating that the Earth has a bulk composition slightly different from all known meteorite groups. Another possibility is that some of the Si may be present in the core, resulting in a bulk silicate Earth having a high Mg/Si ratio.

Table 2.3. CI chondrite and model primitive mantle compositions

		CI chondrite[1]	Primitive Mantle[2]			CI chondrite	Primitive Mantle
Li	ppm	1.5	1.6	Pd	ppb	560	3.9
Be	ppm	0.025	0.068	Ag	ppb	199	8
B	ppm	0.87	0.3	Cd	ppb	686	40
C	%	3.45	0.012	In	ppb	80	11
N	ppm	3180	2	Sn	ppb	1720	130
F	ppm	60.7	25	Sb	ppb	142	5.5
Na	ppm	5000	2670	Te	ppb	2320	12
Mg	%	9.89	22.8	I	ppb	433	10
Al	%	0.868	2.35	Cs	ppb	187	21
Si	%	10.64	21	Ba	ppb	2340	6600
P	ppm	1220	90	La	ppb	234.7	648
S	ppm	62500	250	Ce	ppb	603.2	1675
Cl	ppm	704	17	Pr	ppb	89.1	254
K	ppm	558	240	Nd	ppb	452.4	1250
Ca	%	0.928	2.53	Sm	ppb	147.1	406
Sc	ppm	5.82	16.2	Eu	ppb	56	154
Ti	ppm	436	1205	Gd	ppb	196.6	544
V	ppm	56.5	82	Tb	ppb	36.3	99
Cr	ppm	2660	2625	Dy	ppb	242.7	674
Mn	ppm	1990	1045	Ho	ppb	55.6	149
Fe	%	19.04	6.26	Er	ppb	158.9	438
Co	ppm	502	105	Tm	ppb	24.2	68
Ni	ppm	11000	1960	Yb	ppb	162.5	441
Cu	ppm	126	30	Lu	ppb	24.3	67.5
Zn	ppm	312	55	Hf	ppb	104	283
Ga	ppm	10.0	4	Ta	ppb	14.2	37
Ge	ppm	32.7	1.1	W	ppb	92.6	29
As	ppm	1.86	0.05	Re	ppb	36.5	0.28
Se	ppm	18.6	0.075	Os	ppb	486	3.4
Br	ppm	3.57	0.05	Ir	ppb	481	3.2
Rb	ppm	2.3	0.6	Pt	ppb	990	7.1
Sr	ppm	7.8	19.9	Au	ppb	140	1
Y	ppm	1.56	4.3	Hg	ppb	258	10
Zr	ppm	3.94	10.5	Tl	ppb	142	3.5
Nb	ppb	246	658	Pb	ppb	2470	150
Mo	ppb	928	50	Bi	ppb	114	2.5
Ru	ppb	712	5	Th	ppb	29.4	79.5
Rh	ppb	134	0.9	U	ppb	8.1	20.3

[1][*Anders and Grevesse*, 1989]
[2][*McDonough and Sun*, 1995]

Summary

In this chapter, we touched on how the Earth was assembled. We investigated two approaches for estimating the bulk composition of the Earth, highlighting the accompanying assumptions and uncertainties. We make use of the fact that the Earth presently consists of a Fe metal core and a silicate outer part, which includes both the present day mantle and the crust. We assumed that for those elements that did not enter the core and stayed behind in the residual silicate outer part, we could use natural mantle peridotites or undifferentiated meteorites to infer the composition of the bulk silicate Earth/primitive mantle. We thus concluded this chapter by establishing the starting point - the undifferentiated silicate Earth. In the next few chapters, we will investigate how the silicate Earth has subsequently unmixed to form the continental and oceanic crusts.

Recommended readings

Alexander, C.M.O.D., A.P. Boss, and R.W. Carlson, The early evolution of the inner solar system: a meteoritic perspective, *Science*, *293*, 64-68, 2001.

McSween, H.Y., Jr., *Meteorites and their parent planets*, 310 pp., Cambridge University Press, Cambridge, 1999.

O'Neill, H.S.C., and H. Palme, Composition of the silicate Earth: implications for accretion and core formation, in *The Earth's mantle: composition, structure, and evolution*, edited by I. Jackson, pp. 3-126, Cambridge University Press, Cambridge, United Kingdom, 1998.

McDonough, W.F., and S.-S. Sun, The composition of the Earth, *Chem. Geol.*, *120*, 223-253, 1995.

Allegre, C.J., *From stone to star: a view of modern geology*, 287 pp., Harvard University Press, Cambridge, 1992.

Jagoutz, E., H. Palme, H. Baddenhausen, K. Blum, M. Cendales, G. Dreibus, B. Spettel, V. Lorenz, and H. Wänke, The abundances of major, minor and trace elements in the earth's primitive mantle as derived from primitive ultramafic nodules, *Proc. Lunar Planet. Sci. Conf.*, *10*, 2031-2050, 1979.

Excercises for Chapter 2

2.1. Briefly define the following terms: *bulk silicate Earth, primitive mantle,* and the *bulk Earth*.

2.2 Figure 2.15 shows that the major-element composition of the bulk silicate Earth does not match that of any of the undifferentiated meteorite clans. What is the underlying assumption in this statement and in Figure 2.15? The striking feature of this figure is that the bulk silicate Earth appears to be depleted in Si relative to the undifferentiated meteorites. For sake of argument, assume that the bulk Earth was created from material with a CI carbonaceous chondrite signature. It has been suggested that some Si may have entered the core if conditions were reducing enough [*O'Neill*, 1991; *Allegre et al.*, 1995; *Gessman et al.*, 2001]. Using the data in Table 2.3, calculate how much Si is missing from the bulk silicate Earth (hint: assume that the Mg/Si ratio of the bulk Earth is identical to that of CI, but that there is no requirement for the absolute Si abundances to be the same). If all of the missing Si is in the core, calculate the concentration of Si metal in the core. An alternative hypothesis is that Si was volatilized before or during accretion of the Earth. Explain why this may or may not be the case.

2.3. In a spreadsheet, normalize the elemental abundances of primitive mantle and CI-chondrites each to Mg (what do the resulting numbers mean?). Using the Mg-normalized values, divide primitive mantle by CI-chondrite and plot the values on a graph in the order of decreasing condensation temperature (Figure 2.13). On this plot, denote which elements are considered refractory, moderately volatile, and volatile. Answer the following questions.

a. What does the slope (e.g., the elemental abundance pattern) say about the Earth?

b. Speculate on why the primitive mantle's V, Cr, Mn and Ni contents are low, despite the fact that they are refractory elements.

c. It is believed that the platinum group elements (Pt, Pd, Ir, Os, Ru, and Rh) are highly siderophile, meaning that they should have been entirely sequestered in the core. In light of the plot you have just created, explain if this statement is consistent with observation. Explain why or why not.

Chapter 3
Differentiation:
Melting the mantle

The Earth today is radially heterogeneous. At its center lies the core, surrounding the core lies the mantle, and at its surface lies the continental and oceanic crust, on top of which lie the atmosphere and oceans, respectively. It is likely that the silicate part of the Earth was more or less homogeneous during the Earth's first ~0.5 Gy as there is little or no evidence for differentiated Earth reservoirs (e.g., crust) this early in Earth's history. In this chapter, we continue developing our theme of a differentiating silicate Earth. We will investigate the first step in differentiating the silicate Earth - partial melting, a process in which a liquid phase is generated and physically separated and chemically differentiated from its solid residue. By differentiation, we mean that the liquid has a composition that differs from the solid residue. There is no doubt that oceanic and continental crusts are the solidified products of partial melting. The presence of lavas at mid-ocean ridges and arcs today provides first hand evidence that somewhere in the mantle, melt is being generated, yet paradoxically, we know from seismic studies that nearly all the mantle is in the solid state[9]. The question that arises is how are partial melts generated in a solid Earth? Answering this question requires that we first introduce geologically relevant phase diagrams, enabling us to understand the conditions favorable for melt formation. We then combine this knowledge with what we know about the thermal state of the mantle in various tectonic settings, allowing us to predict what regions of the mantle are likely to melt. Before we can dive into phase diagrams, we will first develop a conceptual understanding of the basic assumptions and principles behind phase diagrams, that is, equilibrium thermodynamics. In this section, we touch on these principles in a semi-quantitative way, leaving the fully quantitative thermodynamic theory to the next chapter.

3.1. The conceptual theory of equilibrium petrology

One of the goals of a petrologist or geochemist is to define the **state** of a **system**. A system is any definable part of the universe that we are interested in, be it the solar system, the Earth, the ocean, or a cubic centimeter of rock. Everything else in the universe represents the **surroundings** of the system. We can describe the state of any system by measuring a certain number of macroscopic properties within the system. If these measurable properties are not changing, then the system is said to be in an **equilibrium state**. If one of the properties in an equilibrium state is disturbed such that the state is perturbed from equilibrium, the system will ultimately return to equilibrium. Thus, the equilibrium state dictates the macroscopic properties of the system. If the equilibrium state changes to another equilibrium state, the change in properties depends only on the two chosen states and not on the process by which one state changes to the other. Because these properties depend only on the equilibrium state, they are called **state variables**, of which there are two types: **intensive** variables (such as density, temperature, and pressure), which are independent of the size of the system, and **extensive** variables (such as mass), which depend on size. Thus, equilibrium processes are **path-independent**, that is state variables do not retain a history. A simple example illustrates this concept. Take a glass of pure water as a simple system. At room

[9] Liquids do not support shear stresses, hence liquids have zero shear-wave seismic velocities, inconsistent with seismic observations of the Earth's mantle.

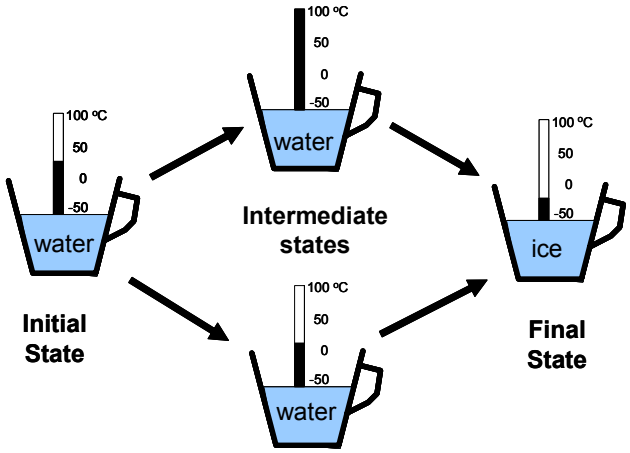

Figure 3.1. The path-independent nature of state variables (in this case temperature). Note that an infinite number of different paths can be taken to convert liquid water to ice, and that water cannot retain a memory.

temperature, this system can be accurately described by temperature, pressure, and density. If we cool the glass of water until it completely freezes, we can measure its temperature, pressure and density at this new equilibrium state. We cannot, however, determine how long or what path it took during its transition between the two equilibrium states (Fig. 3.1). There are an infinite number of paths between the two equilibrium states!

There are, of course, situations in which the process of changing from one equilibrium state to another takes a certain amount of time such that one has enough time to observe and measure the properties of the system during the transition between the two states, or in other words, when the system is in disequilibrium. These processes are said to be **rate-limited**, or **kinetically controlled**, although even when a system is in disequilibrium, various parts of the system can usually be described by **local equlibria**[10]. Thus an olivine phenocryst may be in local equilibrium with the pyroxene that mantles it but not in equilibrium with the host basaltic magma, which is in equilibrium with the pyroxene. Taking our system as the entire magma chamber, the system cannot be said to be in equilibrium even though it can be internally described by a series of local equilibria. In this example, it is the rate-limiting effect of the diffusive mobility of chemical components in olivine, pyroxene and the host melt that retard the attainment of complete equilibrium in the system. By looking at the distribution of certain chemical components in olivine and pyroxene, we may be able to determine how long the magma has been cooling.

In this chapter and the next, we will discuss petrology from the perspective of equilibrium thermodynamics. We will discuss rate-limiting processes, i.e. kinetic theory, in Chapter 11.

3.2. The concept of phases, components and the phase rule

3.2.1 What is a phase?

A **phase** is any physically distinct and homogeneous (in terms of composition and/or structure) portion of a system that can, in theory, be mechanically separated from other phases. For example, a peridotite may consist of the following mineral phases: spinel, olivine,

[10] Philosophically, it can be said that no real system is ever completely in equilibrium as the rate at which a system in disequilibrium attains equilibrium is an asymptotic process.

orthopyroxene, and clinopyroxene. If we were to heat the peridotite to the point at which it first begins to melt, i.e. to generate a liquid phase[11], the partial melt would represent an additional phase along with the four solid mineral phases.

A system that consists of only one phase is said to be a **homogeneous system**, and that consisting of more than one phase is called a **heterogeneous system**. A system containing pure water is an example of a homogeneous system, whereas a typical rock would be an example of a heterogeneous system. A heterogeneous system can be said to be made up of a number of homogeneous sub-systems.

3.2.2 Components

Within any given system, the composition of each phase in the system can be described by the system's **components**, which represent the minimum number of chemical formulae needed to describe each phase. For example, for a system containing only the phases olivine (Mg_2SiO_4), clinopyroxene ($CaMgSi_2O_6$) and orthopyroxene ($Mg_2Si_2O_6$), we can describe each of these phases by simply using MgO, CaO, and SiO_2. We could just as easily use $CaSiO_3$, $MgSiO_3$, and SiO_2 as system components, in which case clinopyroxene = $CaSiO_3$ + $MgSiO_3$, orthopyroxene = $2MgSiO_3$, and olivine = $2MgSiO_3 - SiO_2$. Any additional formulas cannot be considered a component as it can be expressed by a linear combination of any three of the existing components. As there is no unique choice of system components, petrologists typically choose the set of components that is most convenient. For example, the component set $CaSiO_3$-$MgSiO_3$-SiO_2 is awkward in that olivine must be expressed as a negative of one of the components (e.g., $2MgSiO_3 - SiO_2$).

3.2.3 The phase rule

In any given system, there are a number of properties (or variables) that can be used to describe each phase in the system. For example, for each mineral phase we can characterize its density, temperature, pressure, composition, thermal conductivity, heat capacity, and so forth. However, many of these variables are dependent on each other, meaning that once a certain number of variables are known, the remaining variables are simultaneously constrained. As will become evident in Chapter 4, the variables needed to describe the system include temperature, pressure, and the chemical potentials of all components in each phase. Chemical potentials are a measure of the free energy associated with each component. At disequilibrium, the chemical potential of a particular component in two different phases will be different and the system will try to return to equilibrium by reducing the difference between the chemical potentials in the two phases. At equilibrium, the chemical potentials of a particular component are equal in all phases, so the number of unknown chemical potentials is equal to the number of components. We will expand on this notion in more depth in the next chapter, but this feature implies that the number of variables required to describe the system is $c + 2$, where c represents the number of components and the extra two unknowns represent pressure and temperature. Mathematically speaking, we know that if there are n unknowns, then n equations are needed to fully constrain the system. If there are not enough equations, then the system is said to be under-constrained. Thus, a system of n unknowns and $n-1$ equations has one degree of freedom, or in other words, one variable will always remain unknown. In the case of a rock, we will show in the next chapter that each phase defines an equation relating all the variables within a phase to each other.

[11] A liquid is a substance that does not have long-range crystalline order and resistance to shear.

If we let p represent the number of phases in a system, it follows that the degree to which the system is constrained is given as follows:

$$F = c + 2 - p \qquad \text{Eq. 1}$$

Where F represents the **variance** or **degrees of freedom**, c is the number of components, and the value of 2 accounts for the unknown variables, P and T. When $F=0$, the system is described as being invariant, that is, all the variables, including P and T are defined. When $F=1$, the system is called univariant, when $F=2$ the system is called divariant and so forth. In the following sections, we will discuss how the phase rule can be used to study geologic processes.

3.4. Phase diagrams

For any equilibrium system described by a certain number of intensive variables (e.g., T, P, and bulk composition), it is theoretically possible to determine the number of system phases and their proportions. It follows that we can map out phase proportions as a function of these intensive variables, generating what is called a **phase diagram**. Phase diagrams can be theoretically constructed from thermodynamic principles and known thermodynamic parameters, or from experiments in which the intensive variables of interest are controlled. In the latter, the petrologist attempts to simulate in the lab various conditions in the Earth. In the former, one uses tabulations of thermodynamic parameters, which are in turn determined from laboratory experiments.

Here, we will discuss phase diagrams constructed from simple laboratory experiments, leaving the thermodynamic approach until the next chapter. The most useful phase diagrams for the earth scientist are P-T phase diagrams or T-X and P-X phase diagrams, where X represents the compositional variable[12]. We begin with idealized systems in which natural rocks are approximated by just a few components. Nature is obviously more complex than this as there are many more components if all the minor and trace elements are included. Recalling the phase rule from section 3.2.2, it is clear that if all of these components are considered, our system would have an enormous number of degrees of freedom because typical rocks only have a few phases. Fortunately, 99% of the Earth can be described in terms of only 8 elements (see section 1.2), and in fact, a typical rock can be largely described by only 5 components – MgO, CaO, Al_2O_3, SiO_2, and FeO. All other components are in minor or trace amounts, and while such components do in detail effect the properties of a system, we assume first that consideration of only the major components provides a fairly good approximation of a system's properties. Once we understand these so-called simplified systems, we can then begin investigating natural systems.

We begin with the simple case of unary P-T diagrams for systems consisting of one component. For systems with more than one component, additional compositional variables are introduced, so that it is possible to construct phase diagrams in P-X and T-X spaces, as well as P-T space. For these multi-component systems, we begin with isobaric T-X phase diagrams. Then by combining different isobaric sections, we will construct P-T phase diagrams.

3.4.1 Unary system

The system Al_2SiO_5 represents a simple unary system because at geological conditions, the system phases can all be described by one component, Al_2SiO_5. Figure 3.2 shows the stability fields in P-T space of the three polymorphs of Al_2SiO_5 – kyanite, sillimanite, and andalusite [*Holdaway*, 1971]. These aluminosilicate phases are commonly found in

[12] Potential phase diagrams can also be made (see Chapter 4).

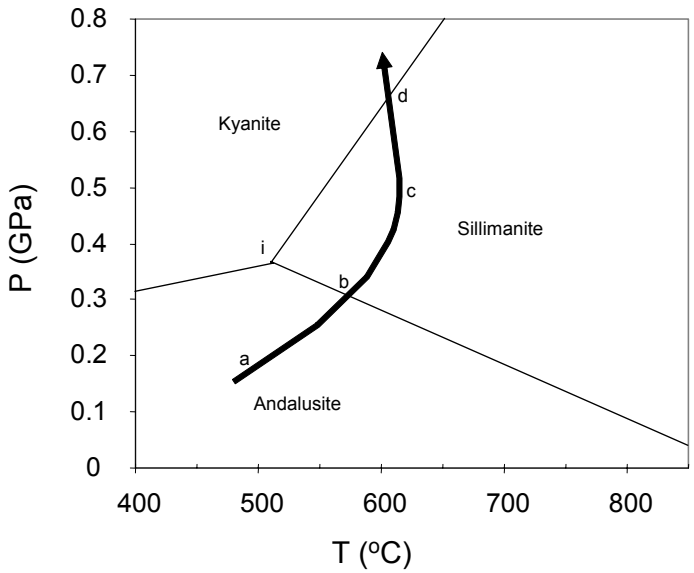

Figure 3.2. Stability of aluminosilicate phases in P-T space for the simple system Al_2SiO_5 [*Holdaway*, 1971]. Arrow represents a hypothetical P-T evolution path.

metamorphosed rocks that had an Al- and Si-rich protolith, such as many sedimentary rocks. They are called polymorphs because each phase is characterized by a different crystal structure even though they have the same mineral formula. It can be seen that the phase diagram in Figure 3.2 can be divided into three regions, in which only one of the phases is stable. These fields are separated from each other by phase boundaries, which are represented by lines in Figure 3.2. At the phase boundary, two phases coexist. At the intersection of the three lines (point *i*), all three phases coexist.

We can gain more insight into how such a phase diagram can help us interpret the P-T conditions at which a rock last equilibrated by applying the phase rule (in the next chapter, we will learn how to construct these diagrams)[13]. This system has one component ($c = 1$), therefore $F = c + 2 - p = 3 - p$, where p is the number of phases. Thus, if we look at a metamorphic rock and find that all three of these aluminosilicate phases coexist (point *i*), we must conclude from the phase rule that $F = 0$, which means that the system-Al_2SiO_5 is invariant. In other words, all the unknowns, that is P, T, and composition (obviously, in unary systems, composition is known), are fixed. There is only one point in P-T space (point *i*), where these three phases coexist, hence, their coexistence in any rock provides a strong constraint on the P-T conditions at which the host rock formed. On the other hand, if the rock is found to contain only two coexisting phases, then the phase rule requires that $F = 1 + 2 - 2 = 1$, and the system is said to be univariant (e.g., points *b* and *d*). This means that there is one free variable, such that the only constraint on P and T in such a system is given by the phase boundary in P-T space (again composition is fixed in this one component example). Thus, if we could independently determine the equilibration P of a rock, its equilibration T would be constrained by the phase boundary in P-T space. Lastly, if a rock is found to contain only one aluminosilicate phase, then

[13] Obviously, a typical rock cannot be described by just one component – Al_2SiO_5. However, so long as one of the phases of these aluminosilicate polymorphs is present in a rock, we can apply this phase diagram by assuming that the aluminosilicate minerals within a rock represent one system. The host rock can then be considered as a larger system, which includes the aluminosilicate system. If the entire rock system is in equilibrium, then all sub-systems within the rock must also be in equilibrium.

the phase rule requires that $F = 1 + 2 - 1 = 2$, and this one-component system is said to be divariant. In this case, both P and T would be independent of each other.

3.4.1 Binary systems

3.4.1.1 Complete solid solution in binary systems

A binary system in which both components mix completely with each other is said to exhibit complete solid solution. Figure 3.3 illustrates a phase diagram in T-X space in the system MgO-FeO-SiO_2 at atmospheric pressure (0.1 MPa; [*Bowen and Schairer*, 1935]). This system can be described by two endmember components of olivine: Mg_2SiO_4 (forsterite) and Fe_2SiO_4 (fayalite). Olivine is the most common mineral in the upper mantle and is a common crystallizing phase in basaltic magmas. At low temperatures, crystalline olivine is stable and at high temperatures a liquid (melt) is stable. The boundary between the stability fields of liquid and crystalline olivine is separated by a "forbidden zone" (white region), which is bounded on the high temperature side by the **liquidus** and the low temperature side by the **solidus**. At any given temperature, the liquidus and the solidus define the compositions of the crystalline olivine and melt.

We can better interpret this figure by considering how the system evolves as we increase temperature. Consider a system characterized by 60 wt. % fayalite component. The system's bulk composition is denoted by X_0. At low temperatures, the system is composed of one phase, crystalline olivine. Because this T-X diagram represents an isobaric slice through a P-T-X diagram, the number of unknowns decreases by one, hence, the *isobaric* phase rule is $F = c + 1 - p$. Thus, when only olivine exists, the system is said to be isobarically divariant, that is, both composition (X) and T must be independently constrained to fully describe the system. If we raise *T*, the olivine will eventually meet the solidus at point *S1* at 1400 °C. At this point, the first onset of melt appears, and the system is said to be isobarically univariant. At this first onset of melting, the melt's composition, *L1*, is dictated by the geometry of the solidus and liquidus, thus if *T* is specified, so are the compositions of the melt and solid. If we increase *T* further, the compositions of the melt and solid are constrained to follow the solidus and liquidus curves (e.g., *S1* goes to *S2*, *L1* goes to *L2*). If our system has remained closed, the bulk composition (summation of all phases in the system) must remain constant. Because mass is conserved in this system, the mass proportions of coexisting melt and solid can be determined from the phase compositions and the bulk composition of the system using the **lever rule**. For example, at temperature *T2*, the mass proportion of melt is given by *(X2-S2)/(L2-S2)* and that of the olivine by *(L2-X2)/(L2-S2)*. At the initial onset of melting, T_1, the melt proportion is infinitesimally small, but

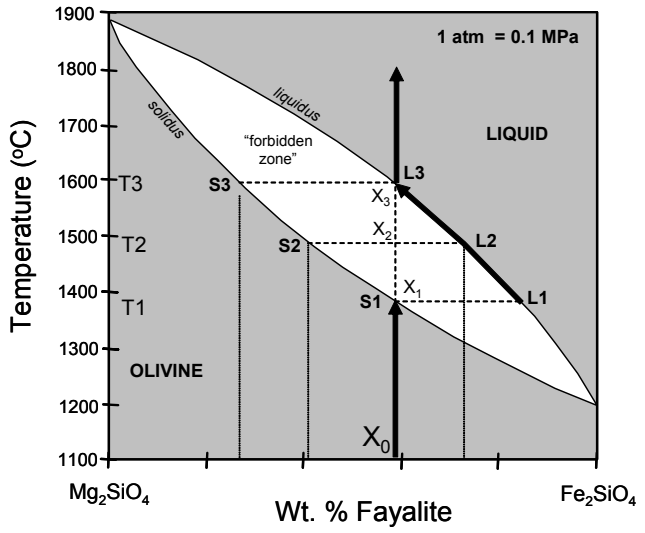

Figure 3.3. Isobaric (1 atm = 0.1 MPa) T-X phase diagram in the system FeO-MgO-SiO_2 exhibiting complete solid solution of Fe and Mg in olivine and in the melt. From [*Bowen and Schairer*, 1935].

as *T* increases, the amount of melt increases at the expense of olivine. Once olivine is exhausted, e.g. at *T3*, the system loses a phase, and as a result, it becomes isobarically divariant. At this point, the system is free to move off the liquidus-solidus join as *T* increases.

3.4.1.2 Eutectics in binary systems – congruent melting

We now consider the case in which there is no solid solution, but there is a low point on the liquidus, called a eutectic. We will use the system $CaMgSi_2O_6$-$CaAl_2Si_2O_8$ as an analog of a basaltic magma at low pressures (clinopyroxene and plagioclase). A diagram from [*Bowen*, 1915] is shown in Figure 3.4. The solid phases in this system are anorthite ($CaAl_2Si_2O_8$) and diopside ($CaMgSi_2O_6$), located at opposite ends of the diagram. Consider the system with bulk composition X_0. At temperatures below 1290 ^oC, the system is composed of two solid phases (anorthite and diopside) and is hence isobarically univariant ($F = c + 1 - p = 2 + 1 - 2 = 1$). If we increase temperature to the point at which a melt phase just begins to appear, i.e. at temperature *T1*, the system will be composed of three phases and will be isobarically invariant, that is, *T* and the composition of all the phases are fixed. The composition of the melt is given by *L1* and the point in the T-X diagram, where all three phases coexist is called the **eutectic**. The important feature to note is that the composition of the eutectic melt can be expressed as some mixture of the original solid mineral phases. This is called **congruent melting**.

Because the system is isobarically invariant at the eutectic, it is not possible for the melt composition to change until there is an additional degree of freedom. Thus, as we heat the rock up in this example, we find that diopside reacts with anorthite to form melt at the eutectic:

$$CaMgSi_2O_6 + CaAl_2Si_2O_8 = \text{melt} \qquad \text{Eq. 3-1}$$

When diopside is exhausted, *F* is equal to 1, and so with continued heating, the melt is allowed to move away from the eutectic point by following the anorthite liquidus towards liquid composition *L2* at the expense of anorthite. During this time, the system is isobarically univariant. When anorthite is finally exhausted, the system becomes isobarically divariant and the melt is allowed to leave the liquidus line and enter the melt-only stability field.

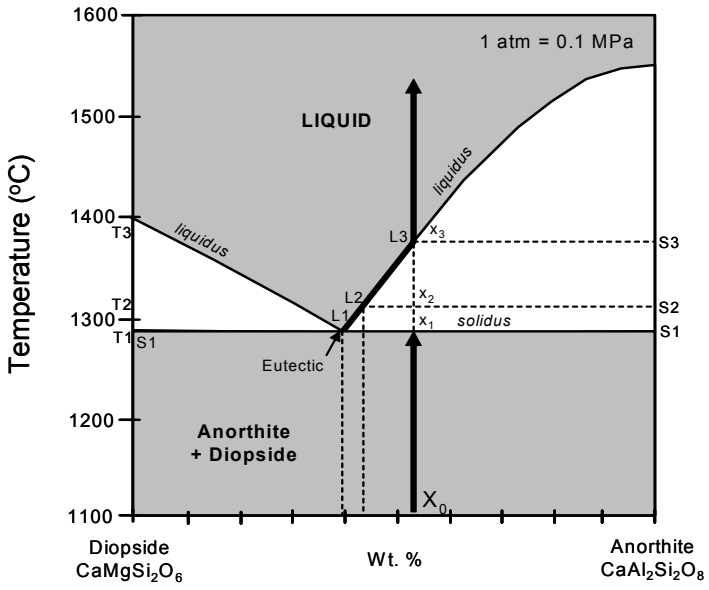

Figure 3.4. A simple analog for basalt at atmospheric pressures using the system diopside-anorthite [*Bowen*, 1915].

Note that we could also reverse our temperature path, such that instead of heating the system, we start off with a melt of bulk composition X_0 and isobarically cool it so that anorthite is the first mineral to crystallize, followed by the co-crystallization of anorthite and diopside. For a closed system, the sequence of equilibrium crystallization reactions would thus be exactly the reverse of the partial melting path shown

in Figure 3.4. This crystallization path is referred to as the **liquid line of descent**.

3.4.1.3 Peritectics in binary systems

Figure 3.5 shows the system Mg_2SiO_4-SiO_2 at atmospheric pressure after [*Bowen and Anderson*, 1914] and can be taken as a simplified analog of a primitive basaltic magma. An inflection in the liquidus line can be seen at point *Pe*, and a third, intermediate phase, enstatite ($MgSiO_3$), is also present. This point is called a peritectic.

We will consider the cooling of magma of bulk composition X_0 in a closed system (equilibrium crystallization). Partial melting is left as an exercise. X_0 lies to the left of enstatite. The magma cools along the liquid line of descent shown by the red arrow in Figure 3.5. As the melt cools, the first mineral to crystallize is olivine (forsterite) at temperature T_1. As the system cools further, the liquid descends along the liquidus, becoming richer in SiO_2 as more olivine crystallizes. At temperature T_{Pe}, the liquid reaches the peritectic point, whereby olivine reacts with the liquid to form orthopyroxene:

$$Mg_2SiO_4 + \text{melt} = 2MgSiO_3 \qquad \text{Eq. 3-2}$$

At this point, there are 3 phases, so the system becomes isobarically invariant ($F = 2 + 1 - 3 = 0$). Only until all of the melt is consumed at T_{Pe}, is the system free to continue decreasing in temperature. The system eventually cools to a subsolidus assemblage of olivine and enstatite.

If instead, we take a magma with bulk composition X_1, lying to the right of the enstatite divide, the following sequence of reactions will occur. Olivine will still be the first to crystallize. When the peritectic point is reached, the olivine back-reacts with the liquid (resorbed) to form

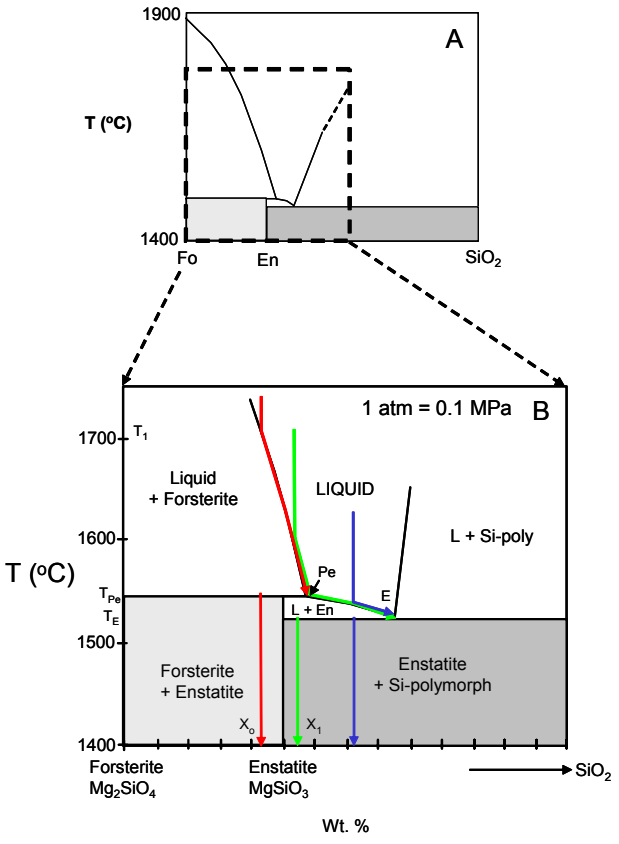

Figure 3.5. Isobaric (1 atm = 0.1 MPa) T-X phase diagram in the system Mg_2SiO_4-SiO_2 after [*Bowen and Anderson*, 1914].

enstatite. When all of the olivine is consumed, the system is composed of melt and enstatite only. As the system cools, the melt follows the enstatite-melt liquidus line until it reaches the eutectic point, where enstatite reacts with the melt to create cristobalite, a SiO_2 polymorph. When all of the melt is consumed, the system is free to crystallize cristobalite and enstatite. This phase diagram shows that olivine and quartz can never coexist in equilibrium because olivine would react with quartz to produce enstatite.

Now, let's consider the reverse – melting of a system having bulk composition X_0, that is, a mixture of enstatite and olivine. The first melt to form will be at the peritectic at T_{PE}. This melt, however, has a composition that is not a simple mixture of the starting phases forsterite and enstatite because the melt is more silicic than both mineral phases. This sort of melting is termed **incongruent melting**.

3.4.2 Melting in a ternary system

We now add an additional component to our system so that we now have a ternary system. The isobaric phase rule in a ternary system is given as $F = c + 1 - p = 4 - p$. Thus, an invariant point consists of 4 phases, an univariant point consists of 3 phases, and so forth. Figure 3.6 shows the 3-component system forsterite-anorthite-quartz (Mg_2SiO_4-$CaAl_2Si_2O_8$-SiO_2) at atmospheric pressure (0.1 MPa) after [*Anderson*, 1915]. The system approximates natural systems as it includes CaO, MgO, Al_2O_3, and SiO_2. Expressed in pure oxide form, this system is strictly speaking a 4-component system, or quaternary system (Figs. 3.6 and 3.7). However, for the phases of interest (forsterite, anorthite, quartz, and enstatite), we can describe all of these phases using the above three components, and hence, we have what is called a pseudo-ternary system. Of course, there are other common phases that can exist in the CaO-MgO-Al_2O_3-SiO_2 (e.g., CMAS) system, such as diopside ($CaMgSi_2O_6$), but in the system Mg_2SiO_4-$CaAl_2Si_2O_8$-SiO_2, diopside does not exist (Fig. 3.6).

The system forsterite-anorthite-quartz represents a rough approximation of basaltic magmas and their ultramafic source regions. The only major component missing is Fe. For basaltic systems, however, the effect of Fe on phase stability and melt compositions is known to be smaller than that of Ca, Mg, Al, or Si, as evidenced by the fact that the FeO contents of basaltic magmas and their solid residues in the mantle are very similar and vary little.

Figure 3.6a represents the liquidus surfaces in this system. Each liquidus surface represents a divariant field in which two phases (liquid and a solid phase) coexist. Each face of the ternary diagram (e.g., the anorthite-quartz, forsterite-quartz, and anorthite-forsterite joins) represents a binary phase diagram. Thus, the forsterite-quartz join is identical to Figure 3.5. The isobarically univariant boundary between two liquidus surfaces is represented by a line, where three phases coexist. Lines connecting to a eutectic are called **cotectics**, and lines connecting to a peritectic are called **peritectics** (Fig. 3.6).

Let us use Figure 3.6 to predict the series of reactions that would take place upon melting a solid with bulk composition X_0, lying to the left of the enstatite-anorthite divide. Such a bulk composition would approximate the mantle at atmospheric conditions[14], which consists of peridotite (see Fig. 2.5 and Table 2.1). We can see that at sub-solidus conditions, this bulk composition consists of forsterite, anorthite and enstatite in the ratio ~27:18:55 %. There is no quartz because it would react with forsterite to form enstatite (see Fig. 3.5 also). If we raise the temperature of the rock, the anorthite reacts with the forsterite and enstatite at the peritectic point to produce a melt incongruently (denoted by the isobaric invariant point having a temperature of

[14] This is of course unrealistic because the pressure in typical mantle conditions is ~1 GPa (atmospheric conditions are 0.1 MPa).

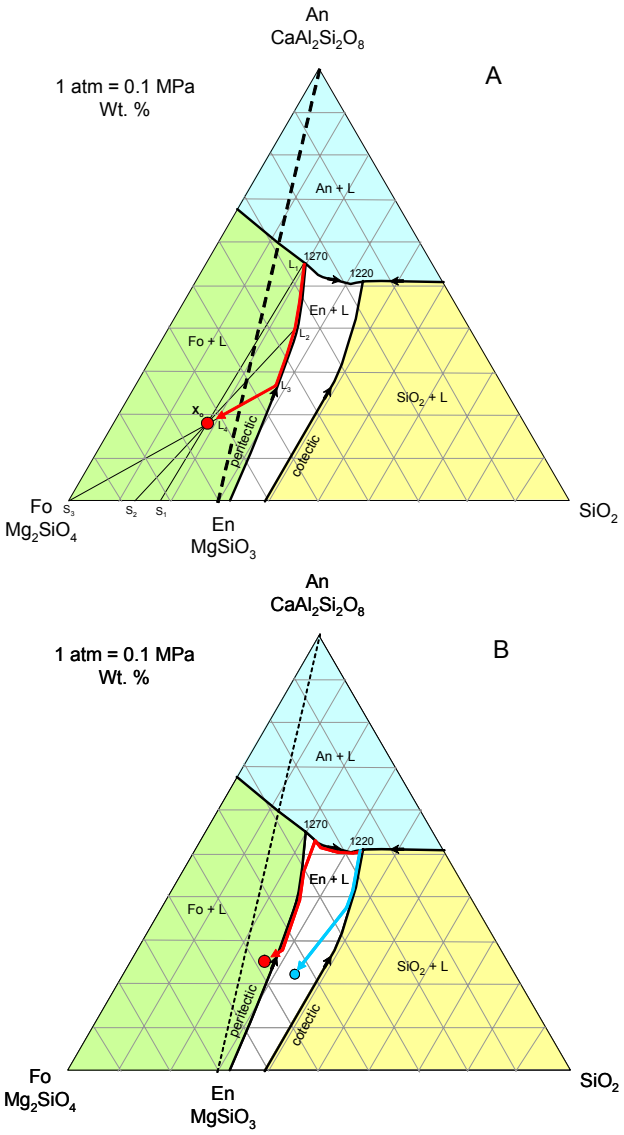

Figure 3.6. Ternary phase diagram in the system forsterite-anorthite-quartz (Mg_2SiO_4-$CaAl_2Si_2O_8$-SiO_2). Fig. 3.6a shows the melting path of a peridotite with bulk composition of X_o, located to the left of the enstatite ($MgSiO_3$) – anorthite join. Fig. 3.6b shows the melting paths taken for bulk compositions that lie to the right of enstatite-anorthite join. Hatched intervals are at 10 wt. % increments.

1270 ^oC). This melt, L_1, will have a composition defined by the peritectic point, and as can be seen, the melt is richer in An and SiO_2 content than the bulk system. When anorthite is completely consumed, the system degrees of freedom increases and the melt is allowed to leave the invariant point. Thus, as temperature increases further, the melt ascends the forsterite-enstatite peritectic line, during which forsterite reacts with enstatite to produce more melt. As the proportion of solid decreases, we also find that the proportion of forsterite relative to enstatite increases, or in other words, with increasing melt fraction, the solid residue becomes more dunitic. Recall that this is exactly what we see in natural peridotites (Fig. 2.5). Thus, when the melt has reached point L_2, the solid residue moves toward S_2. The proportion of melt L_2 is given

by dividing the length of the X_o-S_2 join by the length of the L_2-S_2 join. The ratio of enstatite to forsterite in the solid residue is given by the length of the Fo-S_2 join divided by the En-S_2 join. We can see that the melt cannot stay on the univariant peritectic line indefinitely because at L_3, enstatite is completely exhausted in the solid residue. This allows the system to become isobarically divariant, and therefore the melt is allowed to move onto the liquidus surface. Thus, with increasing temperature, the melt consumes forsterite and moves in the direction of X_o. When the melt composition reaches X_o, all of the solid residue has been exhausted. The system becomes isobarically trivariant, meaning that the melt can now leave the liquidus surface.

Figure 3.6b shows the path taken by a melt in systems with bulk compositions that lie to the right of the anorthite-enstatite divide. In this case, the melt is allowed to evolve to the eutectic, where Fo, En, An, SiO_2 and liquid are stable. The details of the melt trajectories are left as an exercise.

3.4.3 Melting in a quaternary system

As we add more components to our system, the dimensionality of our phase diagrams becomes more complex, and at some point, it is becomes impractical for us to represent such systems graphically. Quaternary systems represent the limit to which graphical diagrams can be made. Here, we consider the quaternary system CaO-MgO-Al_2O_3-SiO_2 at pressures just above 3.0 GPa (Fig. 3.8) taken directly from [*Milholland and Presnall*, 1998]. We consider the ternary subsystem forsterite-anorthite-quartz (Fig. 3.8). In ternary systems, two-phase fields (liquid + one solid phase) are represented by isobarically trivariant liquidus *volumes*. The boundaries between liquidus volumes are represented by surfaces, which are isobarically divariant. The intersections between these surfaces are represented by lines, which are isobarically univariant. Peritectic and eutectic points are isobarically invariant.

We start off with a subsolidus system having bulk composition X_0. Because X_0 lies within the garnet-diopside-enstatite-forsterite tetrahedron, its subsolidus mineral assemblage is

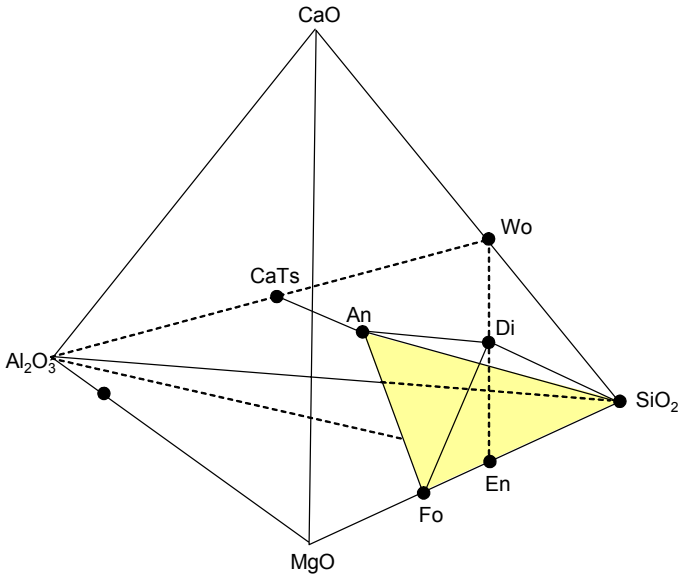

Figure 3.7. The CMAS system (CaO-MgO-Al_2O_3-SiO_2) in weight %. Shaded plane represents the forsterite-anorthite-quartz ternary system shown in Fig. 3.6. Wo = $CaSiO_3$, Di = $CaMgSi_2O_6$, En = $MgSiO_3$, Fo = Mg_2SiO_4, An = $CaAl_2Si_2O_8$, CaTs = $CaAl_2SiO_6$.

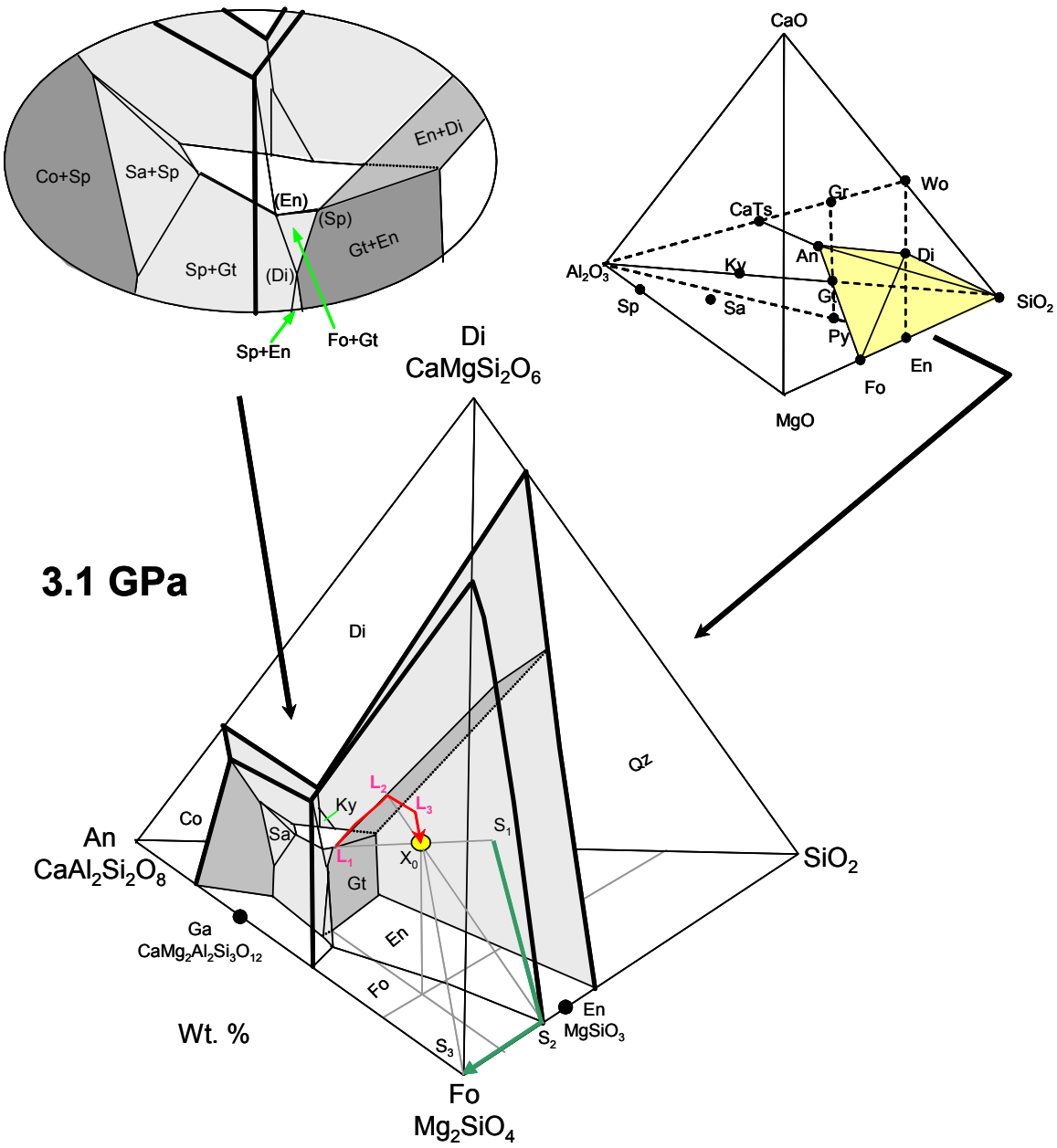

Figure 3.8. Quaternary diagram in the CaO-MgO-Al_2O_3-SiO_2 system, using the Forsterite-Anorthite-Diopside-Quartz subsystem at pressures just above 3 GPa (modified from [*Milholland and Presnall*, 1998]). This corresponds to depths of ~90 km. Symbols are as follows: Wo, wollastonite = $CaSiO_3$; Di, diopside = $CaMgSi_2O_6$; En, enstatite = $MgSiO_3$; Fo, forsterite = Mg_2SiO_4; An, anorthite = $CaAl_2Si_2O_8$; CaTs, Ca-Tschmerakite = $CaAl_2SiO_6$; Ky, kyanite = Al_2SiO_5; Py, pyrope = $Mg_3Al_2Si_3O_{12}$; Gr, grossular = $Ca_3Al_2Si_3O_{12}$; Sa, sapphirine = $Mg_2Al_4SiO_{10}$; Gt, garnet = $CaMg_2Al_2Si_3O_{12}$, Sp, spinel = $MgAl_2O_4$. Yellow circle shows a typical lherzolitic starting composition. Partial melts of this starting composition begin at the diopside-forsterite-enstatite-garnet peritectic (L_1) and follow the diopside-forsterite-enstitate-liquid cotectic to point L_2. When diopside is consumed, the melt can travel along the forsterite-enstatite surface. The composition of the evolving solid residue *in the forsterite-diopside-quartz plane* is shown by the green arrow. With increasing melting, the residue becomes progressively depleted in diopside and enstatite. At L_3 the residue is 100% olivine. Further melting allows the melt to enter the olivine liquidus volume, in which only olivine and liquid are stable.

garnet, diopside, enstatite and forsterite. When the temperature of the system rises to that of the peritectic Gt-Di-En-Fo-L, Gt reacts with Di, En and Fo to create melt of composition L_1. When Gt is exhausted, the system becomes isobarically univariant and therefore the melt is allowed to proceed along the univariant Fo-Di-En cotectic until it reaches a composition of L_2. During this time, the solid residue consists of only Di, En, and Fo, and therefore the composition of the solid residue can be determined from the Di-Fo-SiO_2 plane. The green line shows the evolution of the solid composition (S_1 to S_2) as the melt goes from L_1 to L_2. In Figure 3.8, we can see that at L_2, Di has become completely exhausted, leaving a solid residue containing only En and Fo. The loss of this phase increases the variance of the system, such that the system is now isobarically divariant. This allows it to move along the Fo-En liquidus surface with increasing temperature. The actual path the melt takes on this surface is constrained geometrically by the precipitation of En and Fo. As temperature increases, En becomes progressively exhausted while Fo increases. When En goes to zero, the system's variance increases once again, and the melt is then allowed to move off of the En-Fo liquidus surface and into the En liquidus volume. Its trajectory follows the tieline between Fo and X_0.

This diagram shows that with increasing melting, the solid peridotitic residue is depleted first in garnet, then in clinopyroxene (diopside) and finally in orthopyroxene (enstatite). At very high degrees of melting, the solid residue is pure olivine.

3.5 The effect of pressure on melting

In all of the above examples of phase diagrams, we considered only isobaric sections. This is clearly a simplification of how the mantle really melts because in reality, the system may be undergoing changes in pressure. We can, however, account for the pressure effect in the laboratory by constructing a series of isobaric experiments, and piecing these isobaric phase diagrams together. We will learn in the next chapter that the slope of the liquidus or solidus is almost always positive due to the positive change in molar volume and entropy in going from a solid to a liquid (the ice-water transition is an exception). Thus, with increasing pressure, the point at which a rock begins to melt rises. This can be seen in Figure 3.9 for the diopside-anorthite binary system. The phase diagrams at atmospheric pressures (0.1 MPa) and 1 GPa are shown [*Presnall et al.*, 1978]. Note that the increase in pressure also moves the eutectic to the right, that is, in the direction of the anorthite endmember. This results in an increase in the diopside stability field.

Figure 3.10 shows the olivine liquidus surface in the ternary system anorthite-forsterite-SiO_2 at 3 GPa (~90 km) superimposed on the atmospheric pressure phase diagram (e.g., Fig. 3.6). At 3 GPa, garnet instead of anorthite is the stable aluminous phase. Note that the 3 GPa liquidus field in Figure 3.10 is identical to the projection from diopside in the quaternary system, diopside-anorthite-forsterite-quartz, in Figure 3.8. It can be seen from Figure 3.10, that an increase in pressure results in the peritectic point moving towards the forsterite-anorthite join and increasing in temperature from 1270 ^{o}C at 0.1 MPa to ~1575 ^{o}C at 3 GPa. The former causes the olivine liquidus surface to decrease at high pressure. Thus, if we dynamically change the pressure in a system, we can generate different liquid lines of descent. To illustrate, let's begin with a liquid, L_1, initially in equilibrium with a dunite (e.g., 100 % Fo) in a system with bulk composition X_0 at 3 GPa. As the liquid cools, it follows the 3 GPa En-Fo cotectic, precipitating both Fo and En. Let us allow the liquid to cool to a composition of L_2. If at this point, we suddenly allow the liquid to erupt to the surface of the Earth at rates sufficiently fast that little heat is lost from the liquid to its surroundings, we will find that the liquid now lies above the

olivine stability field despite the fact that it was in the Fo-En-L field at 3 GPa. Upon cooling, this liquid, will precipitate Fo until it hits the An-Fo cotectic, thereby co-precipitating Fo and An. This liquid line of descent is shown by the red arrow in Figure 3.10 and contrasts with the 0.1 MPa liquid line of descent shown by the blue arrow.

By piecing together different isobaric sections determined from laboratory experiments, we can generate a phase diagram in P-T space. Figure 3.11 shows such a P-T diagram generated from a natural peridotite having a bulk composition similar to estimates of primitive mantle (in this case, we have taken the results of [*Takahashi*, 1986], which are based on a commonly used peridotite standard KLB-1). We have chosen a natural peridotite rather than simplified analogues of peridotites (such as the CMAS system in Fig. 3.8) because it is, of course, more

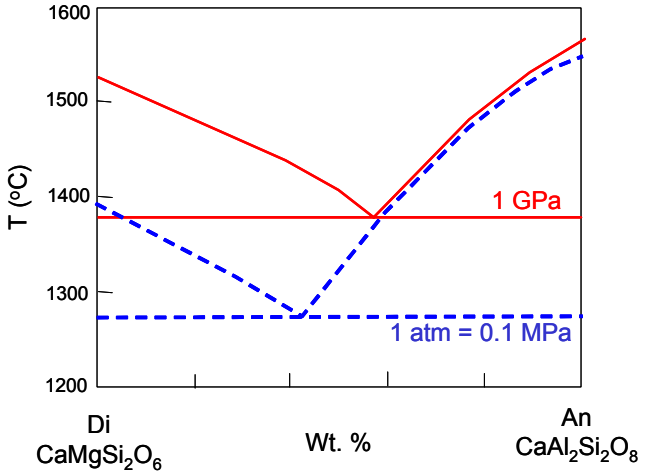

Figure 3.9. The Diopside-Anorthite binary at 1 GPa and 0.1 MPa taken from [*Presnall et al.*, 1978] .

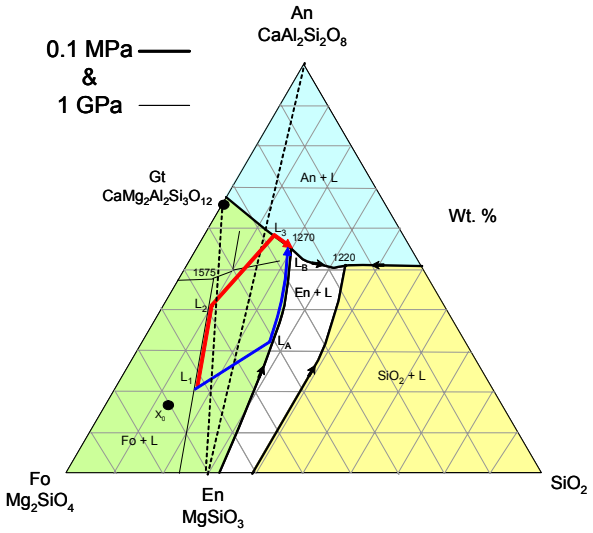

Figure 3.10. The 0.1 MPa and 3 GPa [*Milholland and Presnall*, 1998] ternary phase diagrams in the system Fo-An-SiO_2. Bold lines and colored liquidus surfaces represent 0.1 MPa phase fields as in Figure 3.6. Thin lines represent the 3 GPa phase fields. So as not to clutter the diagram, only the 3 GPa Fo-En cotectic is shown. Blue line represents the isobaric liquid line of descent at 0.1 MPa. The red line represents the formation of a liquid at 3 GPa (L_1 to L_2), followed by sudden decompression to atmospheric pressures (L_2 to L_3).

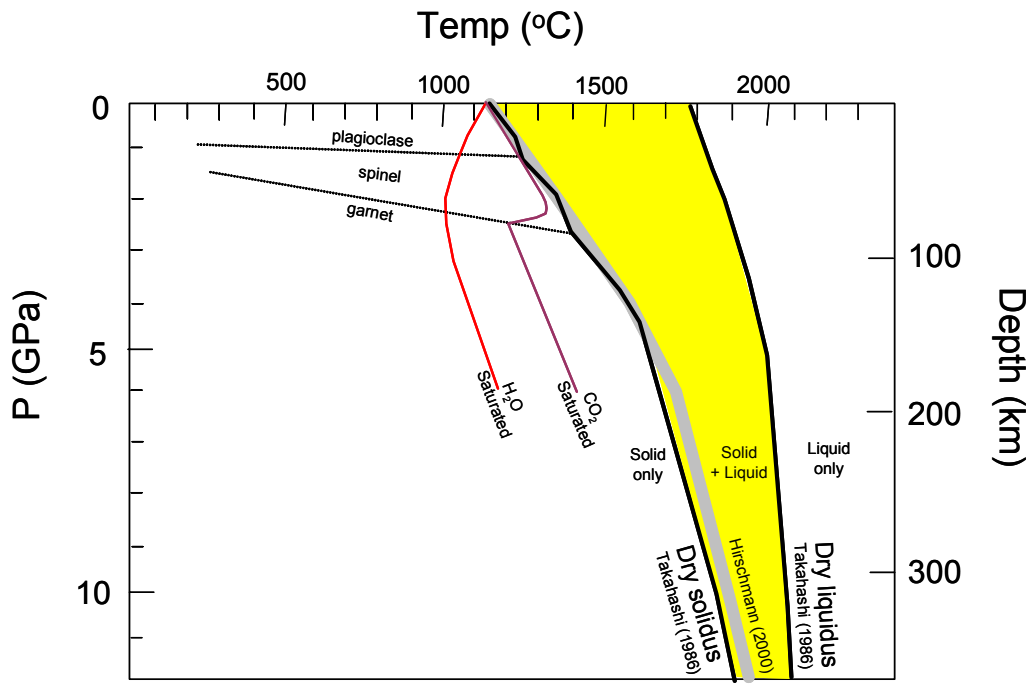

Figure 3.11. P-T phase diagram for a peridotite having a major element composition similar to primitive mantle (see Table 2.1 for primitive value estimates). Thick black lines bounding the yellow region represent melting of a natural peridotite under dry conditions by [*Takahashi*, 1986]. High temperature curve represents the liquidus, which is the point at which solids are completely consumed. Low temperature curve represents the solidus, which is the point at which the first fraction of melt appears. Thick gray line represents the average of a number of solidi compiled by [*Hirschmann*, 2000] from experiments on natural dry peridotites from different laboratories. H_2O and CO_2 saturated curves are from compilation by [*Wyllie*, 1995]. Subsolidus plagioclase-spinel and spinel-garnet transitions are also shown.

applicable to nature. We note, however, that the difference between the solidi and liquidi of natural peridotites and CMAS analogues is small because in the CMAS system, we find that CaO, MgO, Al_2O_3, and SiO_2 account for most of the bulk composition (other than ~8 wt. % FeO). The solidus and liquidus are shown as bold solid lines, bounding a region in which liquid and solid coexist, which is shown by the yellow-shaded region. The solidus represents the point at which the first fraction of melt appears. The liquidus represents the point at which all the solid has been consumed to generate a melt. As can be seen from Figure 3.11, the solidus (and liquidus) have positive P-T slopes. Because melts are generated when a system crosses the solidus in P-T space, we can see that partial melting can occur by heating and/or by decompression. We will see in section 3.7 that this characteristic of the mantle is fundamental to the generation of partial melts in the upper mantle.

3.6 The effect of volatiles on melting

As you probably recognized from the above discussions of multi-component systems, the addition of extra components decreases the melting point of the system. For example, in Figure 3.4, the addition of a diopside component to anorthite, allows a system containing both of these minerals to melt at a lower temperature (the eutectic) than a pure anorthite or pure diopside system. A more familiar analogy is the addition of NaCl to water, which depresses the freezing

point of water. As we will find out in the next chapter, the addition of extra components thermodynamically increases the stability of the liquid phase, allowing the system to commence melting at lower temperatures.

The addition of volatile components, such as H_2O and CO_2, results in the depression of the melting point for the same reason. H_2O- and CO_2-saturated solidi are shown in Fig. 3.11 and compared to the nominally dry peridotite solidus. To the left of these respective solidi, a separate vapor phase exists. In the case of H_2O, there is a separate water phase. In the case of CO_2, either a CO_2 gas phase or a carbonate may exist depending on pressure. To the right of the volatile-saturated solidi, the system is volatile under-saturated, meaning that no separate volatile phase exists. We will return in Chapter 4 to develop a more quantitative and physical understanding of melting point depression by the addition of volatiles. For now, we need only recognize the fact that fluxing of volatiles in the mantle can enhance the production of melt.

3.7 Geodynamic and tectonic controls on melting

In the previous sections, we showed that there are three ways to initiate melting: increasing the temperature, decreasing the pressure, or depressing the solidus by adding water. Here, we discuss how these processes are controlled by geodynamics and tectonic environment. In particular, we attempt below to reconstruct the thermal state of the uppermost mantle so that, when combined with our understanding of relevant phase diagrams, will enable us to determine what regions of the mantle can partially melt.

3.7.1 Heat transfer

The base of the Earth's mantle (core-mantle boundary) is >2000 ^oC, whereas the top of the Earth's mantle, the lithosphere-atmosphere interface is 0-30 ^oC. Common sense dictates that the Earth's mantle wants to cool by releasing heat to the atmosphere and to space. The mantle can cool by conduction and/or by convection. In conduction, heat is transferred by diffusion. An analogy of heat diffusion could be a crowded party in a large room. If the stereo is turned up at one end of the room, the people near it will be energized and begin to dance and bump into each other. By bumping around in place, they will transfer their energy to their neighbors and so forth until the whole floor is dancing (analogous to interactions between vibrating atoms and/or molecules).

An analogy for convective heat transfer would be if we suddenly put a chained (and hungry) tiger at one end of the dance room. Our tiger is the heat source, but the nature of the people near the tiger will change, that is, they will be terrified and have a tendency to run away from the tiger. If they are frightened enough, say if the tiger is a big one, they will be able to push everyone else away as they attempt to run away. These agitated people will eventually reach the far end of the room where their level of agitation will gradually decrease. In turn, the people they have displaced will be get closer to the tiger and become terrified. Thus, so long as our big tiger exists, the people will take turns staying as far away from the tiger as they can. In effect, the people on our dance floor will circulate through, just like a convection cell. Now, let's consider the case in which we replace our tiger with a tiger kitten, which is not too threatening. Under these conditions, there will still be some fear in the people near the kitten, but the fear level will be much less so the tendency to run away will be much less. One might imagine that there is threshold below which the people would rather just dance in place (diffusion) than run away (convection). This threshold is our analog to the Rayleigh number, which denotes the point above which convection initiates.

Now, a more accurate definition of convection is as follows. Let a system (say a box of syrup) begin with a large temperature gradient, such that at the top it is cold and at the bottom it is heated. Because the bottom material is hot, its density is low due to thermal expansion (the people are terrified). This results in a buoyancy force that will provide a tendency to upwell (the tendency for the terrified people to run away). If this buoyancy force can overcome frictional forces resisting its tendency to rise (e.g., viscous forces), it will rise. Thermal convection is thus defined as advection driven by thermal buoyancies. Now, let's follow this hot material that has just upwelled. It will continue to rise so long as it has sufficient thermal buoyancy. However, eventually, our upwelling will have to slow down because it is physically limited by the top of our system. At this point, vertical transfer of heat by advection becomes less efficient and the diffusion of heat (conduction) begins to win out. As heat diffuses out of our system, our upwelled element will become cooler and eventually lose its thermal buoyancy, upon which it will want to sink. This whole cycle is what we call a convective system.

Now, let's return to the question at hand. Does the mantle lose heat by convection or by conduction? We will answer this question in a stepwise manner.

3.7.2 Heat conduction and the thermal boundary layer

Let's begin with the working assumption that the Earth's mantle cools only by conduction and discuss its reasonability. We can derive the heat conduction equation by considering the flow of heat through a small arbitrary cube (Fig. 3.12). In one dimension (x_2-direction), the net heat flow through the faces perpendicular to x_2 is

$$Net\ heat\ flow = \left(q_2 + \frac{\partial q_2}{\partial x_2} dx_2 \right) dx_1 dx_3 - q_2 dx_1 dx_3 = \frac{\partial q_2}{\partial x_2} dV \qquad \text{Eq. 3-3}$$

where q_2 (W/m^2 or J/m^{2}s) represents the heat flux through the left-hand face of the cube perpendicular to x_2 and V represents the volume of the cube. Because energy is conserved, the *net heat flow* from this cube must equal the change in heat content of the cubic volume plus any heat produced (or absorbed) by heat sources within the cube, such as from the decay of radioactive elements. If we denote the heat production function as A (W/m^3) and the change in

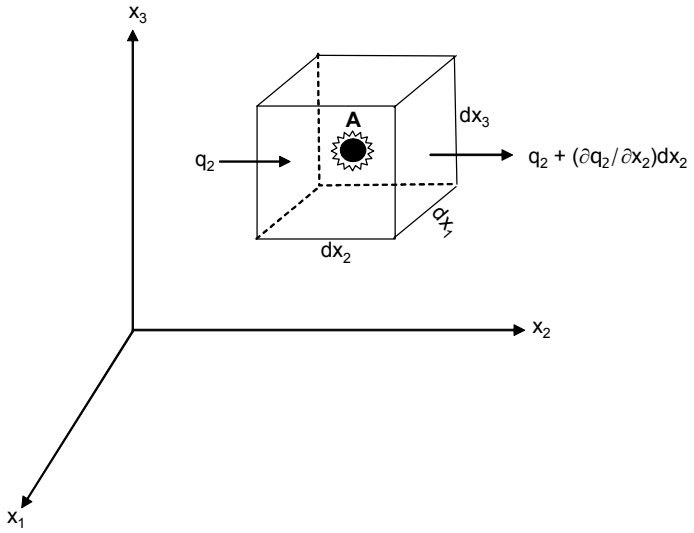

Figure 3.12. Cubic volume *dV* illustrating balance of heat sources. The starred blob in the middle denotes an internal heat source, *A* (W/m^3).

the heat content of the cubic volume dV by $\partial Q / \partial t$ (W), where ∂Q is the change in total heat content (J), the heat balance becomes

$$\frac{\partial q_2}{\partial x_2} dV = -\frac{\partial Q}{\partial t} + A dV \qquad \text{Eq. 3-4}$$

Knowing that the change in heat content is related to the temperature change by

$$\Delta Q = mc\Delta T \qquad \text{Eq. 3-5}$$

where c is the specific heat (J/kg°C) and m is the mass ($m=\rho V$, where ρ is density), and that the flux of heat is related to the temperature gradient by Fourier's law

$$q = -K \frac{\partial T}{\partial x} \qquad \text{Eq. 3-6}$$

where K is the thermal conductivity (W/m°C), Eq. 3-4 becomes

$$\frac{\partial}{\partial x_2}\left(-K \frac{\partial T}{\partial x_2} \right) dV = -c\rho \frac{\partial T}{\partial t} dV + A dV \qquad \text{Eq. 3-7}$$

Dividing by dV and assuming that the thermal conductivity, K, is independent of x, Eq. 3-7 simplifies to the general one-dimensional heat conduction equation

$$\kappa \frac{\partial^2 T}{\partial x_2^2} + \frac{A}{\rho c} = \frac{\partial T}{\partial t} \qquad \text{Eq. 3-8}$$

where the thermal diffusivity $\kappa = K/\rho c$ and has units of m^2/s.

Now, that we have the governing heat conduction equation, we can return to our working assumption that the Earth cools only by conduction. If so, let us assume that the Earth started uniformly hot (~2000 °C) and has since been cooling because its surface is constrained to be cold (~0 °C). We hence have the initial boundary condition, i.e. at time $t = 0$ (beginning of the Earth): $T_{z0}=0\ ^oC$ at depth $z = 0$ and $T_z = 2000\ ^oC$ at all other depths z (black line in Fig. 3.13). The problem that we have just set up is the instantaneous cooling of a uniform infinite half-space. The question that arises is how the temperature profile of this hypothetical Earth has since evolved. For simplicity, let us assume that there is no heat production in the mantle so that $A = 0$. By substitution, we can verify that the following is the solution to Eq. 3-8 (full derivation is given in [*Carslaw and Jaeger*, 1959])

$$\frac{T(t,z) - T_z}{T_{z0} - T_z} = erfc \frac{z}{2\sqrt{\kappa t}} \qquad \text{Eq. 3-9}$$

where *erfc* represents the complementary error function, whose values can be found tabulated in any mathematical tables book. Eq. 3-9 gives the time-dependent evolution of the thermal

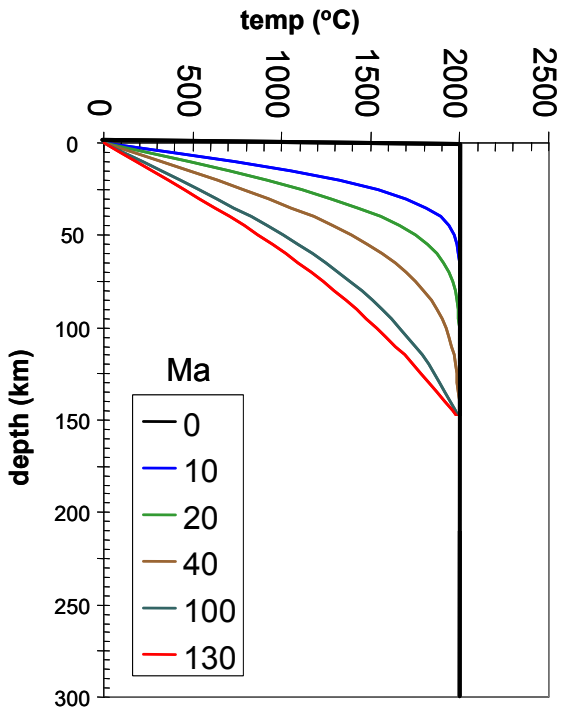

Figure 3.13. Cooling of the Earth assuming heat loss is purely by conduction (κ = 10^{-6}

state of the mantle under pure conduction. Various times steps are shown in Figure 3.13, assuming $\kappa = 10^{-6}$ m^2/s. This figure confirms what your intuition probably told you, that is, the Earth cools gradually from the outside in.

An important feature of Eq. 3-9 is that we can estimate the time it takes for the cooling to propagate into a certain depth z into the mantle. Its thickness at any given time can be approximated by the depth to which the thermal perturbation at the surface boundary has caused a specified perturbation to the initial state. For example, we can define the perturbation depth here to correspond to the depth at which the initial mantle temperature profile has been perturbed by 10%, that is, $\frac{T(t,z)-T_z}{T_{z0}-T_z}=0.1$. Thus, $erfc\frac{z_P}{2\sqrt{\kappa t}}=0.1$ or $erfc^{-1}(0.1)=\frac{z_P}{2\sqrt{\kappa t}}$, where z_P is the propagation depth. As $erfc^{-1}(0.1)$ = 1.16, we find that the propagation depth is

$$z_P \sim 2.32\sqrt{\kappa t} \qquad \text{Eq. 3-10}$$

This simple relationship will time and again prove useful in making back-of-the-envelope calculations on the timescales of thermal and chemical diffusion, so it is worth committing this equation to memory. For example, using a typical rock thermal diffusivity of $\kappa = 10^{-6}$ m^2/s, it can be easily verified from Eq. 3-10 and Figure 3.13 that it takes ~ 180 Ma for the cold front to propagate to depths of ~150 km.

We can now return to the question of whether the Earth cools purely by conduction. Based on seismic data, we know that while the upper thermal boundary layer of the Earth (e.g., the lithosphere) is quite variable, in very few places does it exceed 200 km. Thus, if we take the above reasoning and assumptions at face value, we would have to conclude that the Earth is no more than a few hundred million years old. In fact, the famous physicist Lord Kelvin estimated the age of the Earth by estimating this perturbation depth from the temperature gradient at the surface of the Earth and assuming that the Earth was initially 2000 K[15]. Based on our knowledge of the sedimentary record and radiometric dating, we now know that Lord Kelvin's estimate was far from correct. Lord Kelvin was wrong for two reasons – the presence of radioactive isotopes in the crust and mantle, and perhaps, more importantly, solid-state thermal convection in the mantle (Kelvin, of course, is known for many other great successes and inventions). We will consider radioactivity and convection in the next two sections.

3.7.3 The steady-state conductive geotherm

Let us now return to Eq. 3-8 and make sure to keep the heat production term this time. Let us also assume that the thermal state of the uppermost mantle is at steady state, that is, the temperature and heat flux at any depth z is independent of time t (we will revisit this assumption in the next section). This assumption implies that we have also assumed our heat production term to be time-invariant. Clearly, internal heat generation, if caused by radioactive decay, must itself decay exponentially with time. However, the radioactive decay of the dominant heat producing nuclides (^{238}U, ^{235}U, ^{232}Th, ^{40}K) have half-lives on the order of billions of years and therefore, to first-order, we ignore the time-dependency of heat production[16] as our only goal here is to highlight the effects of heat production on a conductive geotherm. Recognizing these assumptions, Eq. 3-8 becomes

[15] Actually, Lord Kelvin first estimated the age of the Earth to be 65 Ma.

[16] Interestingly, ^{235}U's half-life is about one billion years and so decays on the same timescale as the age of the Earth. Thus, for a full understanding of the Earth's thermal evolution, we indeed have to worry about a decaying heat production term.

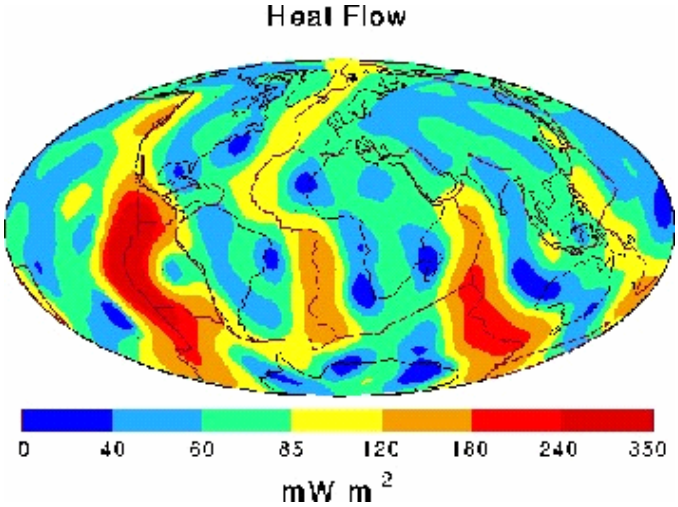

Figure 3.14. Global heat flow map prepared from the database compiled by the International Heat Flow Commission [*Pollack et al.*, 1993].

$$K\frac{d^2T(z)}{dz^2}+A(z)=0 \qquad \text{Eq. 3-11}$$

where A is a function of z only. Eq. 3-11 is a simple 2nd-order ordinary differential equation, which we can solve provided we have the appropriate boundary conditions. The boundary conditions we have are the surface heat flow, q_o, and temperature, T_o, at the surface, $z=0$[17]. For example, Figure 3.14 is a global map of surface heat flow (mW/m^2) taken from [*Pollack et al.*, 1993]. For the case in which A and K are constant, the solution to Eq. 3-11 is

$$T(z)=T_o+\frac{q_o}{K}z-\frac{Az^2}{2K} \qquad \text{Eq. 3-12}$$

The important feature of this solution is that it is a quadratic equation and therefore the shape of *T(z)* is parabolic. The third term on the right, which incorporates the heat production term, introduces a curvature to the steady-state temperature profile, which would otherwise be straight. This is one reason why Lord Kelvin got the age of the Earth wrong (although it is not the main reason, contrary to what many texts lead us to believe).

Eq. 3-12 is obviously simplified as it fails to account for vertical compositional heterogeneity in the upper part of the Earth (A(z)). The main heat-producing elements are U, Th, and K, which generate heat by their radioactive decays. As we will learn later, these elements tend to be enriched in melts, and over the course of Earth's history, they have become highly enriched in the continental crust and correspondingly depleted in the mantle. Accordingly, the heat production in the crust is much higher than that in underlying mantle. To account for this vertical heterogeneity, we can solve Eq. 3-11 by assuming the Earth is composed of a series of homogeneous layers. Then, for each layer, the solution to Eq. 3-11 for the *i*th layer is

$$T_i=T_{oi}+\frac{q_{oi}}{K_i}\Delta z_i-\frac{A_i z_i^2}{2K_i} \qquad \text{Eq. 3-13}$$

[17] The surface heat flow is determined by measuring the thermal gradient dT/dz near the surface of the Earth and the thermal conductivity, K, of the near-surface rocks, and the inserting into Fourier's Law, $q(0)=KdT/dz$.

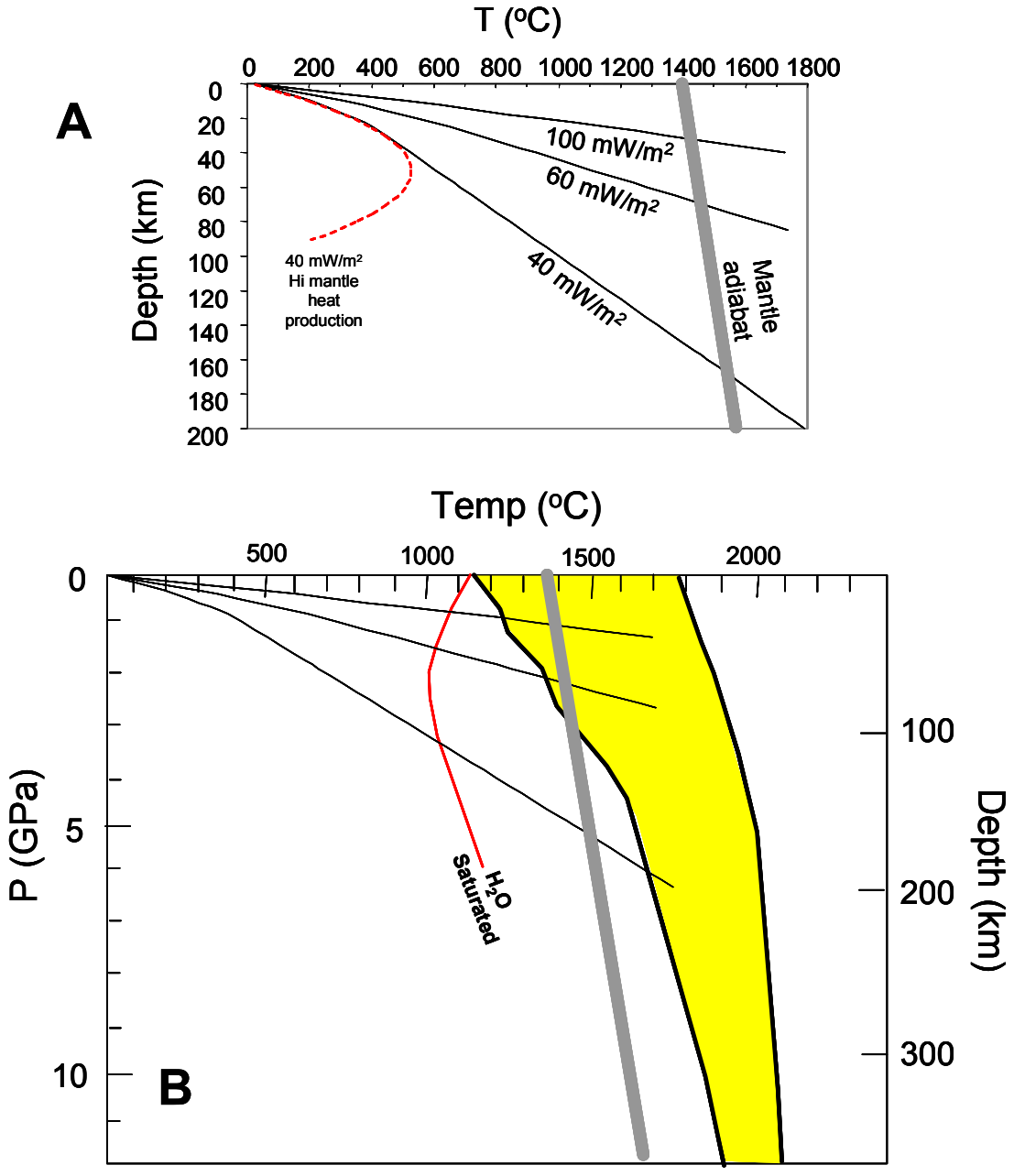

Figure 3-15. a) Various conductive geotherms constrained by the temperature and measured heat flows at the surface of the Earth and by various estimates of the amount of heat production, *A*, in the crust and mantle. All models assume a 30 km thick crust with a constant heat production term of 8×10^{-7} W/m^3. For three of the geotherms (black lines), the mantle has a very small heat production (2×10^{-9} W/m^3). The red dashed curved geotherm represents a 40 mW/m^2 surface heat flow constraint and 8×10^{-7} W/m^3 heat production in the mantle. Mantle adiabat (thick gray line) represents the temperature profile of a vigorously convecting mantle. b) Dry peridotite solidus and liquidus is shown bounding the region of coexisting solid and melt (yellow). The H_2O-saturated solidus is given by the red curve.

where, T_{oi} and q_{oi} are the temperature and heat flow at the top of each layer, A_i and K_i are the heat production and thermal conductivity of the *i*th layer, and Δz_i is the thickness of the layer. Figure 3.15 shows a series of steady-state geotherms for surface heat flow values ranging from 40 to 100 mW/m^2. Surface heat flows of 40 mW/m^2 are characteristic of the old interiors of continents (cratons), while high heat flow regions are characteristic of mid-ocean ridges or highly thinned crust.

It is now worth revisiting our assumptions in assuming that the thermal state of the earth can be described by steady-state conductive geotherms. The steady-state solution to the heat conduction equation, Eq. 3-12, is fully constrained by the boundary condition at the surface of the Earth and estimates of the heat production. If the Earth is losing heat primarily by heat conduction, Eq. 3-12 provides us with the thermal state of the Earth. However, a closer look at Figure 3.15a or Eq. 3-12 indicates the following: 1) if heat production is zero (*A=0*), temperatures will be predicted to increase with depth indefinitely; and 2) if heat production is non-zero, the temperature-depth profile will be parabolic, exhibiting a maximum in temperature at some depth (in Fig. 3.15a, this maximum is seen only for large *A*) followed by a decrease in temperature. Our intuition tells us that temperature cannot increase indefinitely with depth (e.g., Fig. 3.15b) because most of the mantle would be completely molten and we know from seismic studies that this is not true. Similarly, our intuition also tells us that the temperature-profile is not likely to turn around at depth because, if this were so, heat would be flowing into the Earth.

The answer to our problem is that the loss of heat from the Earth is not purely by conduction. The cooling of the Earth occurs instead by convection. Vertical transfer of heat in the interior of the Earth occurs by buoyant upwelling. When upwelled mantle reaches the surface of the Earth and has nowhere to go, it spreads laterally and, in so doing, vertical transfer of heat gradually transitions to a more conductive regime. This transitional regime at the surface is the upper thermal boundary layer. To a certain extent, its uppermost part can be approximated by conductive cooling. However, beneath the thermal boundary layer, vertical transfer of heat is by upwelling.

3.7.4 *Convection and the mantle adiabat*

3.7.4.1 Convection

We now address the question of why the mantle convects. We have all experienced convection at some point in our lives. For example, when one heats a pot of water, we know that the water at the bottom of the pot heats up first, and then, because of its low density, it rises to the top of the pot. Once at the top, it releases heat to the surface by conduction, after which it becomes cooler and denser, sinking back to the bottom of the pot to be heated once again.

To see how this really works, let us look at a tank of a viscous fluid, such as corn syrup (Figure 3.16)[18]. We will investigate the physics of convection from simple dimensional analysis rather than developing the full convective equations. Let's define a spherical volume of corn syrup at the base of the tank. We will refer to this spherical volume as the "blob" from hereon. Let the bottom of the tank be heated and the top of the tank kept at a constant cool temperature. If our blob at the bottom of the thank is heated by ΔT (step A in Fig. 3.16), thermal expansion will cause its density, ρ, to decrease by

$$\Delta\rho = -\rho_o \alpha \Delta T \qquad \text{Eq. 3-14}$$

[18] This dimensional analysis approach was inspired by one of Richard J. O'Connell's undergraduate courses at Harvard University.

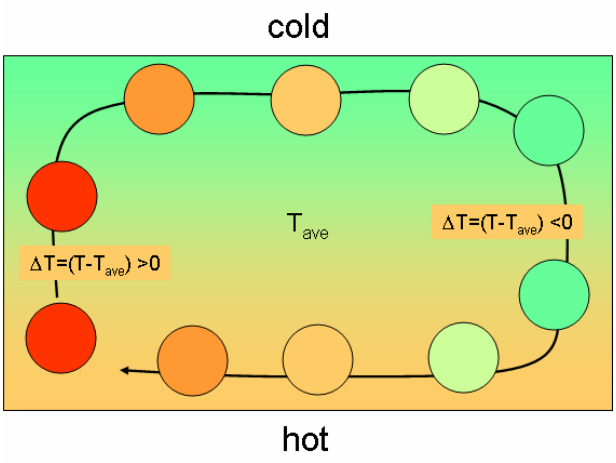

Figure 3-16. A schematic diagram illustrating the concept of convection. A heated water balloon in an aquarium.

where α is the thermal expansivity ($^oC^{-1}$) of the corn syrup and ρ_o (kg/m^3) its density prior to being heated. The resulting low density will result in a buoyant force, F_B (kgm/s^2), on the blob

$$F_B = \frac{4}{3}\pi R^3 \Delta\rho g = \frac{4}{3}\pi R^3 \alpha \rho_o \Delta T g \qquad \text{Eq. 3-15}$$

where R is its radius and g is the gravitational acceleration (9.8 m/s^2)[19]. This buoyant force will be counteracted by a drag force, F_D, which is the viscous resisting force from the surroundings. To first approximation, the drag force is given by the shear stress, τ (force/area), times the surface area of the blob

$$F_D = 4\pi R^2 \tau \qquad \text{Eq. 3-16}$$

In a viscous fluid, the shear stress is given by

$$\tau = \eta \dot{\varepsilon} \qquad \text{Eq. 3-17}$$

where η is the viscosity (Pa s) and $\dot{\varepsilon}$ is the strain rate (s^{-1}), which represents a measure of the rate of deformation. If we can approximate the strain rate as

$$\dot{\varepsilon} = U / R \qquad \text{Eq. 3-18}$$

where U is the upwards velocity of the blob and R is the approximate distance into the surrounding fluid that is deformed by the movement of the blob, then Eq. 3-16 becomes

$$F_D = 4\pi R^2 \tau = 4\pi R \eta U \qquad \text{Eq. 3-19}$$

If we assume that F_D=F_B, we can solve for the *approximate* upwards velocity of the blob owing to thermal expansion:

$$U = \frac{\Delta\rho g R^2}{3\eta} \qquad \text{Eq. 3-20}$$

Eq. 3-20 is an *approximate* form of the "Stoke's settling velocity" (although in this case, it is the rising velocity) derived from dimensional analysis. The actual velocity is given by

$$U = \frac{2\Delta\rho g R^2}{9\eta} \qquad \text{Eq. 3-21}$$

[19] What would happen if there was no gravity?

Our simplified velocity is off from the true velocity by only a small factor. If we insert the effect of thermal expansivity, Eq. 3-21 becomes

$$U = \frac{2\alpha\rho_o g\Delta T R^2}{9\eta} \qquad \text{Eq. 3-22}$$

Eq. 3-22 shows that the upward velocity of the blob is directly proportional to the square of its radius and to the density contrast between it and its surroundings. In contrast, it is inversely proportional to the viscosity of the surrounding fluid.

Now, let us assume that once our heated blob leaves the bottom, it has left its heat source. Our blob will now have the chance to cool by losing heat to its surroundings (e.g., by conduction). If it cools, its thermal buoyancy will decrease and it will rise less slowly. Our intuition tells us that if the blob rises too slowly, it will lose its heat to its surroundings and the blob will not upwell significantly. On the other hand, if the blob rises rapidly compared to the loss of heat, it will retain its thermal buoyancy and continue to rise. Convection commences. There is thus a critical threshold at which convection begins. Recall from section 3.7.2 that we derived an approximate relationship between the time and distance of thermal propagation by conduction of heat (Eq. 3-10). Using Eq. 3-10, the approximate time, t_{th}, it takes for the blob to cool off is then given by

$$t_{th} = R^2 / 4\kappa \qquad \text{Eq. 3-23}$$

If we denote the point at which the blob starts to rise by the point at which it rises by a distance R, then the rise time, t_B, is given by

$$t_B = R / U \qquad \text{Eq. 3-24}$$

If $t_B < t_{th}$, then the blob rises and convection begins. If $t_B > t_{th}$, then the blob cools off before having a chance to rise; heat will be transferred by conduction rather than by convection. The tendency for convection should thus scale according to the dimensionless ratio t_B/t_{th}:

$$t_{th} / t_B = \frac{\alpha\rho_o g\Delta T R^3}{18\kappa\eta} \qquad \text{Eq. 3-25}$$

Except for a constant, this dimensionless ratio is very similar to the more rigorously derived **Rayleigh number**, which is the ratio of buoyancy forces to viscous resisting forces, and thus is a measure of the tendency for a system to convect. For a bottom heated layer, the Rayleigh number is given by

$$Ra = \frac{\alpha\rho_o g\Delta T L^3}{\kappa\eta} \qquad \text{Eq. 3-26}$$

where L is the thickness of the layer and ΔT is the temperature difference between the top and bottom. From laboratory and numerical experiments, fluid dynamicists have shown that convection will occur if Ra exceeds the critical Rayleigh number, Ra_c, which is on the order of 10^3. Eq. 3-26 shows that a large layer thickness and a large temperature difference favors convection. As expected, high viscosity and high thermal diffusivity counteract convection because the former resists flow and the latter dissipates heat, which decreases thermal buoyancies. Depending upon what one assumes to be the scale of convection in the mantle, the mantle's Rayleigh number is on the order of 10^5 to 10^7, indicating that the mantle convects! Given that a typical thermal expansivity is 3×10^{-5} $^oC^{-1}$, the viscosity of the mantle is of the order 10^{20} to 10^{21} Pa s, and the thermal diffusivity of typical rocks is of the order 10^{-6} m^2/s, we leave the verification of this conclusion to the reader.

3.7.4.2 The mantle adiabat

Let us return to our previous discussions about the thermal state of the Earth. We now know that the Earth is convecting. The uppermost part of the Earth is made up by the upper thermal boundary layer of the Earth's convection cell. Its thermal state can be approximated by conductive heat loss. So what is the temperature profile in the upwelling (or downwelling) portion of the Earth's interior? Let's assume the mantle upwells rapidly such that no heat is lost from an upwelling volume to its surroundings (e.g., no conductive loss), that is, an "adiabatic" process. If no heat is lost, we might then expect there to be no change in temperature. It turns out that we are almost correct. The temperature change is indeed very small. In detail, however, there is a small decrease in temperature during upwelling due to decompression. This is because as the mantle upwells, decompression leads to expansion, which causes the upwelling mass to perform work on the surroundings, resulting in a slight decrease in its internal energy (or temperature). Conversely, adiabatic compression is accompanied by work being done on the downwelling mass, which increases its internal energy and hence temperature. The temperature profile for adiabatic decompression (or compression) is termed the **adiabat**. The isentropic adiabatic temperature gradient with pressure at any given pressure is given by

$$\left(\frac{\partial T}{\partial P}\right)_S = \frac{\alpha T}{\rho C_p} \qquad \text{Eq. 3-27}$$

where C_P is the specific heat (J/kg^{o}C) at constant pressure, α is the thermal expansivity, g is gravity, T is temperature and P is pressure. Eq. 3-27 can be re-expressed in terms of temperature versus depth (z) by assuming that the Earth is lithostatic, that is, $dP = d(\rho g z) = \rho g dz$, where we have assumed that the reference density ρ is constant over reasonable depth ranges (if there are phase transitions, this is of course not valid). Plugging this expression for pressure into Eq. 3-27 gives the temperature-depth gradient at a given depth:

$$\left(\frac{\partial T}{\partial z}\right) = \frac{\alpha g T}{C_p} \qquad \text{Eq. 3-28}$$

Now, let us see what the average adiabatic temperature gradient in the Earth is. To do this, let's ignore the Earth's lithosphere, which is where vertical heat transport occurs primarily by conduction of heat. To do this, we need to assume that the upwelling mantle just beneath the mid-ocean ridge has a temperature of ~1350 ^{o}C (1623 K), the thermal expansivity of most rocks is ~3 x 10 $^{-5}$ ^{o}K^{-1} and the heat capacity is 1 kJ kg^{-1} ^{o}K^{-1}. Keeping track of units, we see from Eq. (13) that the adiabatic temperature gradient in the uppermost mantle is roughly 0.5 ^{o}C/km, which is small compared to the temperature gradient seen in the thermal boundary layer. To calculate the adiabatic temperature profile as a function of depth, we need only integrate Eq. 3-28:

$$T(z) = T_o \exp\left(\frac{\alpha g}{C_p}(z - z_o)\right) \qquad \text{Eq. 3-29}$$

Where T_o is the temperature at a given reference point z_o. If z_o is set to zero, then T_o is called the **potential temperature**. This is the temperature that mantle would be if it were adiabatically decompressed all the way to the surface of the Earth. It is of course a fictive number because heat is lost by conduction in the upper thermal boundary layer. It is, however, used as a common reference point whenever one talks about the "temperature of the mantle".

3.7.5 Synthesis – melting the mantle

Now that we have a better understanding of the mantle's thermal state, let us return to the question of what makes the mantle melt. We can use Figure 3-17 to guide us. The first point to

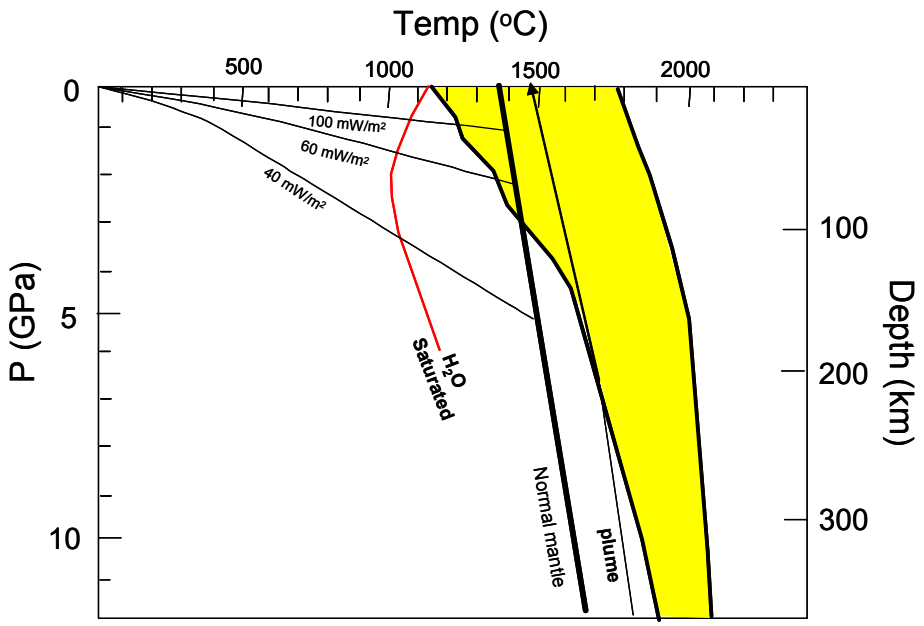

Figure 3-17. Same as in Figure 3-16, except that temperature-depth paths of upwelling mantle beneath mid-ocean ridges (normal mantle) and in plumes are shown.

recognize from Figure 3-17 is that the melting occurs where the geotherms intersect the mantle solidus. Let us first assume that the temperature profile of the mantle is approximated by piecing together the steady-state conductive geotherm with the mantle adiabat. Then for a dry mantle, Figure 3-17 shows that the geotherm for the 100 mW/m^2 surface heat flow intersects the dry peridotite solidus at ~1 GPa, or 30 km. If we look at Figure 3-14, we see that surface heat flows of 100 mW/m^2 or greater occur only at or near mid-ocean ridges, and indeed, partial melting occurs beneath mid-ocean ridges. By contrast, the geotherm for a 40 mW/m^2 surface heat flow, which is characteristic of the old interiors of continents, never intersects the mantle solidus, implying that partial melting does not occur beneath continental interiors. This is also consistent with the general observation that magmatism is absent in the interiors of continents.

We can also see from Figure 3-17 that we can induce melting at lower temperatures if we flux the mantle with water. It can be seen that if the mantle is water saturated, then partial melting may occur in any of the thermal conditions shown in Figure 3-17. Depression of the solidus by the addition of water is what allows melting to occur above subducting slabs, which flux the overlying mantle wedge with water. More on water later.

We can also see from Figure 3-17 that the slope of the mantle adiabat is not as steep as the mantle solidus, so the mantle adiabat intersects the solidus. Thus, as portions of the mantle upwell, decompressional partial melting occurs when the adiabat crosses the solidus. Decompressional melting for the case of normal mantle (i.e. beneath mid-ocean ridges) is shown as a thick solid arrow. Decompressional melting can also occur for plumes, in which the potential adiabat temperature is much higher. In such cases, partial melting commences at greater depths, allowing higher degrees of partial melting. Given this information, it follows that any form of adiabatic decompression can give rise to partial melting if the solidus is crossed. Thus, partial melting can be initiated when crust is rapidly thinned, either by extension or by sudden removal ("delamination") from the lower part of the lithosphere.

Summary

In this chapter, we discussed the basic concepts of partial melting. In multi-component systems, the melting point is depressed. We then discussed the stability of melt and solid phases as a function of bulk composition, temperature and pressure with the aid of experimentally constrained phase diagrams. The temperature-pressure slope of the peridotite solidus was shown to be greater than that of the mantle adiabat. In addition, we showed that the addition of volatile components, such as H_2O and CO_2, further depresses the peridotite solidus. Partial melting can thus occur by an increase in temperature, by adiabatic decompression, or by the depression of the solidus by the addition of water. These processes can occur in a variety of tectonic environments, depending upon the background thermal state. Regions of high heat flow, such as mid-ocean ridges and highly extended continental crustal regions, are characterized by geotherms with steep temperature gradients such that the base of the thermal boundary layer lies well within the partial melting P-T field. In this case, partial melting occurs where the mantle adiabat intersects the solidus. Regions characterized by low heat flow, such as the stable interiors of continents, are not prone to melting as these "cold" geotherms never intersect the mantle solidus. Partial melting of the mantle wedge overlying subducting slabs occurs because the peridotite solidus has been depressed by the addition of volatiles.

Derivation of adiabatic temperature gradient

Eq. (12) can be derived more rigorously by manipulating various thermodynamic equations. One way is to call upon the total differential of entropy S with respect to T and P:

$$dS = \left(\frac{\partial S}{\partial T}\right)_P dT + \left(\frac{\partial S}{\partial P}\right)_T dP \tag{1}$$

We must then make use of the following definitions

$$\left(\frac{\partial S}{\partial T}\right)_P = \frac{c_p}{T} \tag{2}$$

where c_p in this case represents the molar heat capacity in $J\ mol^{-1}\ ^oK^{-1}$,

$$\left(\frac{\partial S}{\partial P}\right)_T = -\left(\frac{\partial V}{\partial T}\right)_P = -\alpha V \tag{3}$$

where V is now the molar volume (m^3/mol). For an isentropic process, $dS = 0$. Thus, upon rearranging Eq. (15), we arrive at

$$\left(\frac{\partial T}{\partial P}\right)_S = \frac{\alpha V T}{c_p} \tag{4}$$

and if we divide the numerator and denominator by the gram formula weight (e.g., mass of one mole of the substance of interest), we arrive at

$$\left(\frac{\partial T}{\partial P}\right)_S = \frac{\alpha T}{\rho C_p} \tag{5}$$

where C_p is the heat capacity expressed in terms of $J\ kg^{-1}\ ^oC^{-1}$.

Exercises for Chapter 3

1. Refer back to Figure 3.6b. Using the phase rule, rationalize the equilibrium melting paths for the two systems whose bulk compositions lie to the right of the En-An join. Explain the sequence in which mineral and melt phases appear or disappear. In so doing, quantitatively show how the phase proportions evolve with increasing degree of melting (*Hint: it may be more intuitive to follow a liquid line of descent, which in a closed system in complete equilibrium, will be exactly the reverse of the partial melting path*).

2. Tracking phase proportions during equilibrium closed system melting in the binary Forsterite-SiO_2 system (Fig. 3.5). Using the bulk compositions given in Fig. 3.5, make a graph of mineral phase proportions as a function of temperature.

3. For the Forsterite-Fayalite binary and the Diopside-Anorthite binary, show how the paths of equilibrium and fractional crystallization might differ. To do so, choose the same starting composition for the melts in both cases. In the case of equilibrium closed system crystallization, the composition of the system is the original starting composition of the melt and must remain constant. For fractional crystallization, assume that as soon as a mineral is precipitated from the melt, it is instantaneously taken out of the melt. Thus, the composition of the system is continually changing owing to the loss of crystals. Now, try plotting the reverse of crystallization, that is, the paths for equilibrium and fractional melting.

4. A basaltic magma intrudes as a dike into granitic country rock. Upon intruding, it entrains pieces of granitic fragments. If the dike width (*2L*) is 4 m, estimate how long it will take for the dike to cool to the temperature of its surroundings (use a thermal diffusivity κ of 10^{-6} m^2/s). If the average granitic fragment has a radius of 5 cm, how long does it take to heat such a fragment to the temperature of the host basalt? If the granitic fragment becomes completely molten, it can be incorporated into the basaltic magma either by physical mixing and stirring, or by chemical diffusion. If the propagation distance of chemical diffusion is given by $x = \sqrt{4Dt}$ where *D* the chemical diffusivity (m^2/s), calculate approximately how long it takes for the basalt and granitic melt to become homogenized by diffusion alone (assume that the main component in granite is Si, which has a chemical diffusivity of 10^{-13} m^2/s). How does this timescale compare to the lifespan of the dike?

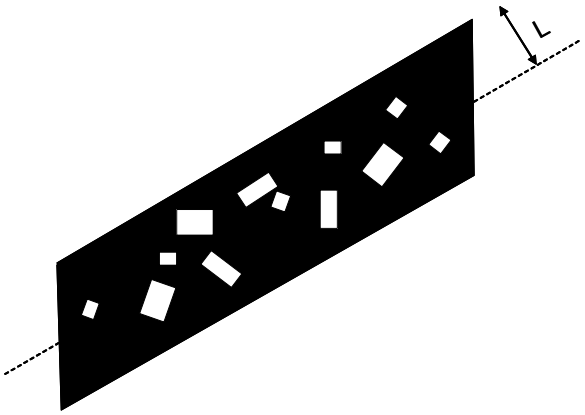

Figure 3-18. A basaltic magma intrudes as a dike (black) and entrains fragments of granitic country rock (white).

6. Return to Figure 3.6a. Calculate the wt. % of oxides (e.g., MgO, CaO, Al_2O_3, SiO_2) in the peritectic melt L_1 and the bulk system X_0. Compare and contrast the two compositions.

7. If the temperature in the upwelling mantle at 100 km depth is 1450 ^oC, what is the potential temperature? If thermal expansivity of mantle rocks just happened to be zero, what would the adiabatic temperature gradient be? Would the mantle convect at all?

8. Consider the following cases for an intrusion of basaltic magma. A) a sill of thickness 10 m and B) a magma chamber of thickness 200 m. Which, if any, will undergo convection?

9. Recall from Chapter 2 and Figure 2.5 that with increasing degrees of partial melting, the solid peridotite residue becomes richer in olivine mode and obtains a higher Mg# (100 × molar Mg/(Mg+Fe)). In some rare situations, melt-depleted peridotites appear to have excess orthopyroxene, or equivalently an olivine deficit, for a given Mg# as shown in Figure 3-18a and b. One explanation for this is that a silicic melt, perhaps derived from melting of subducted sediments or oceanic crust, infiltrated and reacted with the melt-depleted peridotites to generate excess orthopyroxene [*Kelemen et al.*, 1998]. This two-step process is an example of **modal metasomatism**. Let us use the phase diagram in the ternary Fo-Di-SiO_2 system at 2.0 GPa in Figure 3-18c to see how this process works. We assume for simplicity that the addition of FeO has a minimal effect on the topology of the phase diagram. In the following, we use the terms Fo and olivine, and En and orthopyroxene interchangeably.

   We begin with a highly melt-depleted peridotite (dunite) with composition X_0 (where olivine is represented by Fo = 100%). Let us assume that this dunite represents a piece of the hot asthenospheric wedge lying above a subducting slab. A silicic melt, i.e. one in which quartz is stable, is generated in the subducting slab. Let this melt have composition L_0 (Di = 58%, Fo = 20 %, SiO_2 = 22%). If this melt separates from its source and enters the overlying mantle wedge, it will react with the dunite.

a) If the amount of melt that enters the dunite is such that the **new system** can be described by 40% L_0 and 60% X_0, calculate (graphically) the new bulk composition of the system. Do this by drawing a tieline between X_0 and L_0. Using a ruler and the lever rule, denote the new bulk composition on Figure 3-18c by X_1.

b) Assuming equilibrium, the system phase proportions and compositions will have to change because the bulk composition of the system has changed. Let us assume that the system can equilibrate immediately. If the temperature conditions are such that solid and liquid can coexist, show in the figure the possible range in melt compositions. Show and explain also the possible range of solid compositions (enstatite mode will increase). What are the minimum and maximum proportions of enstatite that can be formed (hint: the maximum enstatite mode is when the reacted liquid just reaches the peritectic Fo+Di+En+L)? For a particular equilibrium assemblage, calculate the proportion of solids and melts using the lever rule. Comment on your results.

c) Assume that the silicic melt that infilitrates into the mantle wedge has 4.4 wt. % MgO and 6.6 wt. % FeO. Verify that its Mg# is ~54 (Mg# = 100 × molar Mg/(molar Mg + molar Fe)). Assume that the dunite has 52.5 wt. % MgO and 6.9 wt. % FeO. Verify that its Mg# is ~93. What we want to calculate is the Mg# of the solids after melt-rock reaction. To do so, we will use the ternary phase diagram in Fig. 3-18; we assume that the addition of FeO does not change the phase diagram significantly.

   i. Calculate the bulk MgO and FeO content of the system where the proportions of L_0 is 40 wt. % and X_0 is 60 wt. %.

   ii. After reaction, take the case with the highest orthopyroxene mode. Calculate the proportions of melt, olivine, and orthopyroxene using the lever rule.

   iii. Let us assume that at equilibrium, MgO and FeO in the melt is proportional to the amount of MgO and FeO in olivine (Ol) and orthopyroxene (Opx), that is,

$$D_{MgO}^{Opx} = MgO^{Opx} / MgO^{melt} = 3.3$$

$$D_{FeO}^{Opx} = FeO^{Opx} / FeO^{melt} = 0.69$$

$$D_{MgO}^{Ol} = MgO^{Ol} / MgO^{melt} = 4.8$$

$$D_{FeO}^{Ol} = FeO^{Ol} / FeO^{melt} = 1.5$$

   where the *D's* represent effective **partition coefficients**. Using the above information, calculate the MgO and FeO content of the melt after reaction by first setting up a mass balance equation:

$$MgO^{BULK} = X^{Opx} MgO^{Opx} + X^{Ol} MgO^{Ol} + X^{melt} MgO^{melt}$$

   where MgO^{BULK} is the wt. % of MgO in the entire system (e.g., the 40%-60% mixture of L_0 and X_0), X^i is the weight fraction of the *ith* mineral phase, and MgO^i is the wt. % of MgO in a particular phase. A similar equation can be written for FeO.

   iv. Now that the MgO and FeO content of the reacted melt has been determined, calculate the MgO and FeO contents of the olivine and orthopyroxenes using the partition coefficients shown above. Use this information to calculate the MgO and FeO content of the solid. What is its Mg#? For this case, plot the Mg# and olivine mode in Figure 3-18a or b.

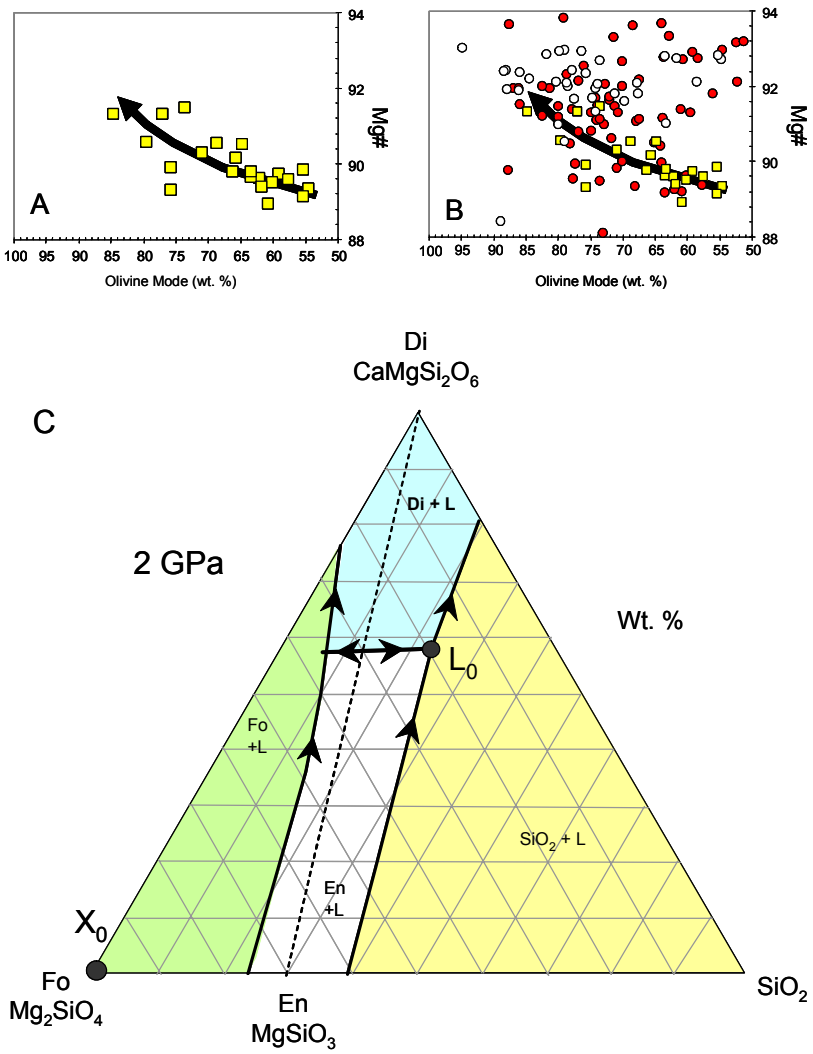

Figure 3-19. a) The effect of melt extraction on the composition of the solid peridotite residue. b) In some samples, there is an excess of orthopyroxene at a given Mg# (or deficit in olivine). Reaction between melt-depleted peridotite and a silicic melt has been suggested to form orthopyroxene at the expense of olivine. c) ternary diagram in the Fo-Di-SiO_2 system at 2.0 GPa from [*Liu and Presnall*, 2000].

Alexander, C.M.O.D., A.P. Boss, and R.W. Carlson, The early evolution of the inner solar system: a meteoritic perspective, *Science*, *293*, 64-68, 2001.
Allegre, C.J., *From stone to star: a view of modern geology*, 287 pp., Harvard University Press, Cambridge, 1992.
Allegre, C.J., J.-P. Poirier, E. Humler, and A.W. Hofmann, The chemical composition of the Earth, *Earth Planet. Sci. Lett.*, *134*, 515-526, 1995.
Anders, E., and N. Grevesse, Abundances of the elements: meteoritic and solar, *Geochim. Cosmochim. Acta*, *53*, 197-214, 1989.
Anderson, O.L., The system anorthite-forsterite-silica, *Amer. J. Sci.*, *39* (407-454), 1915.
Birch, F., On the possibility of large changes in the Earth's volume, *Phys. Earth Planet. Int.*, *1*, 141-147, 1968.
Bowen, N.L., The crystallization of haplodioritic, and related magmas, *Amer. J. Sci.*, *40*, 161-185, 1915.
Bowen, N.L., and O.L. Anderson, The binary system MgO-SiO_2, *Amer. J. Sci.*, *37*, 487-500, 1914.
Bowen, N.L., and J.F. Schairer, The system MgO-FeO-SiO_2, *Amer. J. Sci.*, *29*, 151-217, 1935.
Carslaw, H.S., and J.C. Jaeger, *Conduction of heat in solids*, 510 pp., Oxford University Press, Oxford, 1959.
Elthon, D., High magnesia liquids as teh parental magma for ocean floor basalts, *Nature*, *278*, 514-518, 1979.
Frey, F.A., W.B. Bryan, and G. Thompson, Atlantic ocean floor: geochemistry and petrology of basalts from Legs 2 and 3 of the Deep Sea Drilling Project, *Journ. Geophys. Res.*, *79*, 5507-5527, 1974.
Gessman, C.K., B.J. Wood, D.C. Rubie, and M.R. Kilburn, Solubility of silicon in liquid metal at high pressure: implications for the composition of the Earth's core, *Earth Planet. Sci. Lett.*, *184*, 367-376, 2001.
Green, D.H., The metamorphic aureole of the peridotite at the Lizard, Cornwall, *Journ. Geol.*, *72*, 543-563, 1964a.
Green, D.H., The petrogenesis of the high-temperature peridotite intrusion in the Lizard area, Cornwall, *Journ. Petrol.*, *5*, 134-188, 1964b.
Green, D.H., A re-study and re-interpretation of the geology of the Lizard peninsula, Cornwall, in *Present view on some aspects of the geology of Cornwall and Devon*, pp. 87-114, Royal Geological Society, London, 1964c.
Grossman, L., Condensation in the primitive solar nebula, *Geochim. Cosmochim. Acta*, *36*, 597-619, 1972.
Hart, S.R., and A. Zindler, In search of a bulk-earth composition, *Chemical Geology*, *57*, 247-267, 1986.
Hirschmann, M.M., Mantle solidus: experimental constraints and the effects of peridotite composition, *Geochem. Geophys. Geosys.*, *1*, 2000GC000070, 2000.
Holdaway, M.J., Stability of andalusite and the aluminum silicate phase diagram, *Amer. J. Sci.*, *271*, 97-131, 1971.
Jagoutz, E., H. Palme, H. Baddenhausen, K. Blum, M. Cendales, G. Dreibus, B. Spettel, V. Lorenz, and H. Wänke, The abundances of major, minor and trace elements in the earth's primitive mantle as derived from primitive ultramafic nodules, *Proc. Lunar Planet. Sci. Conf.*, *10*, 2031-2050, 1979.

Kelemen, P.B., S.R. Hart, and S. Bernstein, Silica enrichment in the continental upper mantle via melt/rock reaction, *Earth. Planet. Sci. Lett.*, *164*, 387-406, 1998.
Larimer, J., and E. Anders, Chemical fractionations in meteorites 2: abundance patterns and their interpretation, *Geochim. Cosmochim. Acta*, *31*, 1239-1270, 1967.
Liu, T.-C., and D.C. Presnall, Liquidus phase relations in the system CaO-MgO-Al_2O_3-SiO_2 at 2.0 GPa: applications to basalt fractionation, eclogites, and igneous sapphirine, *Journ. Petrol.*, *41*, 3-20, 2000.
Lodders, K., and J. Fegley, B., *The planetary scientist's companion*, 371 pp., Oxford University Press, Oxford, 1998.
McDonough, W.F., and S.-S. Sun, The composition of the Earth, *Chem. Geol.*, *120*, 223-253, 1995.
McSween, H.Y., Jr., *Meteorites and their parent planets*, 310 pp., Cambridge University Press, Cambridge, 1999.
Milholland, C.S., and D.C. Presnall, Liquidus phase relations in the CaO-MgO-Al_2O_3-SiO_2 system at 3.0 GPa: the aluminous pyroxene thermal divide and high-pressure fractionation of picritic and komatiitic magmas, *Journ. Petrol.*, *39*, 3-27, 1998.
Norton, O.R., *The Cambridge encyclopedia of meteorites*, 354 pp., Cambridge University Press, Cambridge, 2002.
O'Neill, H.S.C., The origin of the Moon and the early history of the Earth-a chemical model. Part 2, the Earth, *Geochim. Cosmochim. Acta*, *55*, 1159-1172, 1991.
O'Neill, H.S.C., and H. Palme, Composition of the silicate Earth: implications for accretion and core formation, in *The Earth's mantle: composition, structure, and evolution*, edited by I. Jackson, pp. 3-126, Cambridge University Press, Cambridge, United Kingdom, 1998.
Palme, H., and K.G. Nickel, Ca/Al ratio and composition of the Earth's upper mantle, *Geochim. Cosmochim. Acta*, *49*, 2123-2132, 1985.
Pollack, H.N., and D.S. Chapman, On the regional variation of heat flow, geotherms, and lithospheric thickness, *Tectonophys.*, *38*, 279-296, 1977.
Pollack, H.N., S.J. Hurter, and J.R. Johnson, Heat flow from the Earth's interior; analysis of the global data set, *Rev. Geophys.*, *31*, 267-280, 1993.
Presnall, D.C., S.A. Dixon, J.R. Dixon, T.H. O'Donnell, N.L. Brenner, R.L. Schrock, and D.W. Dycus, Liquidus phase relations on the join diopside-forsterite-anorthite from 1 atm to 20 kbar; their bearing on the generation and crystallization of basaltic magma, *Contrib. Mineral. Petrol.*, *66*, 203-220, 1978.
Ringwood, A.E., *Composition and petrology of the Earth's mantle*, 188 pp., 1975.
Ringwood, A.E., *Origin of the Earth and Moon*, Springer-Verlag, Berlin, 1979.
Ross, C.S., M.D. Foster, and A.T. Myers, Origin of dunites and olivine-rich invlusions in basaltic rocks, *Am. Mineral.*, *39*, 693-737, 1954.
Rudnick, R.L., Fountain, D. M., Nature and composition of the continental crust: a lower crustal perspective, *Reviews of Geophysics*, *33*, 267-309, 1995.
Takahashi, E., Melting of a dry peridotite KLB-1 up to 14 GPa: implications on the origin of peridotitic upper mantle, *Journ. Geophys. Res.*, *91*, 9367-9382, 1986.
Wänke, H., G. Dreibus, and E. Jagoutz, Mantle chemistry and accretion history of the Earth, in *Archean Geochemistry*, edited by A. Kröner, pp. 1-24, Springer-Verlag, Berlin, 1984.
Wasson, J.T., *Meteorites: their record of early solar-system history*, W. H. Freeman, San Francisco, 1985.

Wyllie, P.J., Experimental petrology of upper mantle materials, processes and products, *Journ. Geodyn.*, *20*, 429-468, 1995.